

Evaluation of a new inference method for estimating ammonia volatilisation from multiple agronomic plots

Benjamin Loubet^{1,*}, Marco Carozzi^{1#}, Polina Voylokov¹, Jean-Pierre Cohan², Robert Trochard², Sophie Générmont¹

1 INRA, UMR ECOSYS, INRA, AgroParisTech, Université Paris-Saclay, 78850, Thiverval-Grignon, France

2 ARVALIS-Institut du Végétal, **Station expérimentale de La Jaillière, La Chapelle Saint Sauveur, 44370 Loireauxence**, France

now at: Agroscope Research Station, Climate and **Agriculture**, Zurich, Switzerland

* Corresponding author: Benjamin.Loubet@inra.fr

Abstract. Tropospheric ammonia (NH₃) is a threat to the environment and human health and is mainly emitted by agriculture. Ammonia volatilisation following application of nitrogen in the field accounts for more than 40% of the total NH₃ emissions in France. This hence represents a major loss of nitrogen use efficiency which needs to be reduced by appropriate agricultural practices. In this study we evaluate a novel method to infer NH₃ volatilisation from small agronomic plots made of multiple treatments with repetition. The method is based on the combination of a set of NH₃ diffusion sensors exposed for durations of 3 hours to 1 week, and a short-range atmospheric dispersion model, used to retrieve the emissions from each plot. The method is evaluated by mimicking NH₃ emissions from an ensemble of 9 plots with a resistance-analogue-compensation-point surface exchange scheme over a yearly meteorological database separated into 28-days periods. A multi-factorial simulation scheme is used to test the effects of sensor number and heights, plot dimensions, source strengths and background concentrations, on the quality of the inference method. We further demonstrate by theoretical considerations in the case of an isolated plot that inferring emissions with diffusion sensors integrating over daily periods will always lead to underestimations due to correlations between emissions and atmospheric transfer. We evaluated these underestimations as $-8\% \pm 6\%$ of the emissions for a typical western European climate. For multiple plots, we find that this method would lead to median underestimations of -16% with an interquartile [-8% -22%] for two treatments differing by a factor of up to 20 and a control treatment with no emissions. We further evaluate the methodology for varying background concentrations and NH₃ emission patterns and demonstrate the low sensitivity of the method to these factors. The method was also tested in a real case and proved to provide sound evaluations of NH₃ losses from surface applied and incorporated slurry. We hence showed that this novel method should be robust and suitable for estimating NH₃ emissions from agronomic plots. **We believe that the method could be further improved by using Bayesian inference and inferring surface concentrations rather than surface fluxes. Validating against controlled source is also a remaining challenge.**

Keywords: NH₃ emission, multiple sources, dispersion modelling, experimental design, diffusive samplers

Introduction

Tropospheric ammonia (NH₃) is mainly emitted by agriculture and has great environmental impacts (atmospheric pollution, eutrophication, reduction of biodiversity) which are increasingly taken into account in

38 European and international regulations (Council, 1996; Council, 2016; UNECE, 2012). Ammonia losses also
39 have great agronomic and economic impacts for farmers, as it reduces nitrogen use efficiency. The varying
40 prices of mineral fertilizers and concerns about environmental and health threats demand improvements in the
41 efficiency of nitrogen utilisation, and especially in recycling nitrogen through organic fertilization (Sutton et al.,
42 2011). Indeed, NH₃ volatilization during storage of manure and slurry and following their field application is the
43 main source of NH₃ in Europe (55% of the emissions) while farm buildings emissions represent **45%**. In
44 **France, crop farming represent 35% of the emission and animal farming represent 65%** (CITEPA, 2017;
45 ECETOC, 1994; EUROSTAT, 2012; Faburé et al., 2011). Reducing NH₃ losses from this agricultural sector is
46 therefore a major objective for applied research.

47 While NH₃ emissions from farm buildings and storage can be handled by engineering solutions, losses during
48 organic fertilisation are much more dependent on the combination of application methods (splash plate, band
49 spreading, pressurised injection, open and close slot injection, trailing hose and trailing shoe), soil type and
50 occupation, and environmental conditions (soil humidity, air temperature, wind speed, solar radiation) (Sommer
51 et al., 2003). For instance, Sintermann et al. (2012) report NH₃ losses following cattle and pig slurry application
52 in the field ranging from a few percent to 50% over large fields and up to 100% over medium fields. Evaluating
53 ammonia losses from field fertilisation over a range of practices, soil and climatic conditions is therefore key in
54 evaluating the best application methods.

55 However, characterising these emissions at the field scale requires complex experimental design and most of the
56 time **also requires the use of** large fields (Ferrara et al., 2016; Ferrara et al., 2012; Flechard and Fowler, 1998;
57 Loubet et al., 2012; Milford et al., 2009; Sintermann et al., 2011b; Spirig et al., 2010; Sun et al., 2015;
58 Whitehead et al., 2008). Especially useful for measuring ammonia losses are methods that can deal with small
59 and medium-scale fields (20-50 m on the side) **that are commonly used in agronomic trials**. Indirect estimation
60 methods (soil nitrogen balance or ¹⁵N balance) are not well adapted to evaluate gaseous ammonia losses, mainly
61 because of the soil heterogeneity and also because the method relies on evaluating small variations of large
62 numbers (McGinn and Janzen, 1998). Among existing methods for measuring NH₃ emissions, the integrated
63 horizontal flux method (Wilson and Shum, 1992) is well adapted, but is a subject of debate in its practical
64 application since it seem to be systematically biased towards higher estimates (Häni et al., 2016; Sintermann et
65 al., 2012). Alternatively, enclosure methods proved to be not representative for a sticky compound such as
66 ammonia (Pacholski et al., 2006), but more concerning is the fact that ammonia fluxes result from an air-surface
67 equilibrium which is disturbed by the confined environment offered by the chamber. Inverse dispersion
68 modelling approaches either based on backward Lagrangian Stochastic models (Flesch et al., 1995) or Eulerian
69 models (Kormann and Meixner, 2001; Loubet et al., 2001), based on the Philip equation (Philip, 1959) have
70 been demonstrated to be adapted for estimating NH₃ volatilization from **strong** sources (Loubet et al., 2010;
71 Sommer et al., 2005).

72 These approaches are well adapted to small or medium fields ($\leq 50 \times 50$ m²) but typically require hourly **NH₃**
73 **concentration measurements**. Long term concentration measurements of NH₃ are now well handled by the use
74 of short path passive samplers developed by Sutton, et al. (2001), or active denuders, which have both been used
75 for concentration monitoring for years (Tang et al., 2001; Tang et al., 2009). These active denuders can be
76 adapted for measuring fluxes based on conditional sampling like the conditional time averaged gradient method
77 COTAG (Famulari et al., 2010), which is a useful method but only adapted for large fields (≥ 0.5 ha). The

78 passive samplers have also been shown to be adapted for inverse modelling estimations of NH₃ sources for large
79 fields (Carozzi et al., 2013b; Ferrara et al., 2014).

80 | In another field of research, solutions to the multiple source **inference** problem, which consists of inferring
81 multiple sources based on measured concentrations at multiple points in space and time, have been developed
82 especially since 2008 (Crenna et al., 2008; Gao et al., 2008; Gericke et al., 2011; Mukherjee et al., 2015; Vandré
83 and Kaupenjohann, 1998). They have chiefly been used over regional scales (Flesch et al., 2009; Lushi and
84 Stockie, 2010; Yee and Flesch, 2010), and have been shown to be very dependent on the source-sensor geometry
85 (Crenna et al., 2008; Flesch et al., 2009; Wang et al., 2013). Mukherjee et al. (2015) highlighted the dependency
86 of the inferred source to background concentration and plot disposition, by means of an inverse footprint
87 approach. Yee et al. (2008) have shown how to retrieve the number, location and intensity of multiple sources
88 with dispersion models coupled with Bayesian inference methods. Yee and Flesch (2010) have evaluated the
89 inversion and inference methods for determining 4 points sources using several laser transects. Flesch et al.
90 (2009) have shown that source-receptor geometry is critical in determining whether a multiple-source inversion
91 problem can provide realistic solutions or not. Flesch et al. (2009) have moreover shown that if the geometry is
92 | well chosen the accuracy of the method for 15 min **integration time** can reach 10% to 20%. These studies have
93 also shown that the multiple source **inference** problems can be solved if not ill-conditioned (ill-conditioning
94 depends on the location of sources and concentration sensors and is characterised by a conditioning number κ).

95 In this study, we pose the following research questions: **“Can inverse dispersion modelling approaches be
96 used for inferring NH₃ emissions from multiple small plots (agronomic trials) using passive samplers, and
97 to which degree of accuracy?”** The answer is given through the investigation of the optimal design in terms of
98 | field dimensions, plots **location** and size, passive sampler locations and their duration of exposure. Throughout
99 this study, agronomic trials are considered as adjacent multiple small fields with repetitions of treatments. A
100 typical trial would consist of three repetitions of three treatments. Hence the double challenge that we face in this
101 | study is (i) to consider together the multiple source **inference** issue (adjacent small fields) and the (ii) time-
102 integration issue (using passive samplers).

103 To answer these questions, we use a 4 step approach: (1) The ammonia emissions are first modelled on each
104 source using prescribed NH₃ emission potential dynamics coupled with a simple soil-vegetation-atmosphere
105 exchange scheme to mimic realistic seasonal, daily and hourly variations in NH₃ emissions. (2) These prescribed
106 emissions are then used to estimate the concentration at each target location using short-range atmospheric
107 dispersion modelling over half hourly periods. (3) The obtained concentrations are then averaged over several
108 integration periods to simulate the behaviour of passive samplers. Finally, (4) the sources are evaluated by
109 inference with dispersion modelling based on the averaged concentrations.

110 Two dispersion models and several inference methodologies are evaluated. The effect of the size of the source,
111 | the locations of targets, the dynamics and magnitude of each source, the meteorological conditions **and the
112 background concentration variability** are evaluated and discussed. The feasibility of the method is finally
113 evaluated over a real case with two repetitions of three treatments (slurry spreading, injection and a reference
114 without fertilisation).

115 2. Materials and methods

116 At first we present the theoretical background of source inference by optimisation for single and multiple sources
117 with time averaging concentration sensors. Then the method used to generate a realistic ammonia source is
118 **introduced before** the **description of the** dispersion models used for **both** generating the concentration fields
119 and inferring back the sources. The geometry of the sources, **sensor locations** and the meteorological data used
120 **for this analysis** are then shown, and finally the real test case used for evaluating the method is detailed.

121 2.1 The theory of the source inference method

122 At first we will recall some important theoretical features of the inverse dispersion modelling approach which is
123 actually an inference method.

124 2.1.1 Case of a single area source and a single concentration sampler

125 We first consider the case of a single area source with a single concentration sampler (target). The source is
126 varying with time. The method is based upon the general superimposition principle (Thomson et al., 2007),
127 which relates the concentration at a given location $C(x,t)$ to the source strength $S(t)$ and the background
128 concentration $C_{bgd}(t)$ using a transfer function $D(x,t)$, which has the dimensions of a transfer resistance ($s\ m^{-1}$).

129

$$130 \quad C(x,t) = D(x,t) \times S(t) + C_{bgd}(t) \quad (1)$$

131

132 Here x denotes the location of the sensor and t the time. **The concentration and source units are in μg**
133 **$\text{N-NH}_3\ \text{m}^{-3}$ and $\mu\text{g N-NH}_3\ \text{m}^{-2}\ \text{s}^{-1}$, respectively.** The superimposition principle implies that the studied tracer
134 must be conservative, which is a reasonable hypothesis for NH_3 whose reaction time with acids in the
135 atmosphere is below the transport time for spatial scales below 1000 m (Nemitz et al., 2009). Moreover, in **Eq.**
136 **(1)**, we assume a spatially homogeneous area source with strength $S(t)$. The spatial homogeneity of the source is
137 less trivial for NH_3 **than other gas released in agriculture** as the source itself depends on the concentration at
138 the surface. However (Loubet et al., 2010) have shown that the heterogeneity of the source can be neglected as
139 long as the dimension of the source is larger than 20 m. Hence, this study is limited to source areas with fetch
140 larger than 20 m and a spread of the concentration samplers over a domain smaller than 1000 m. Moreover, it is
141 interesting to note that for infinitely spread fields, the transfer resistance is linearly linked to the transfer matrix
142 (see supplementary material S1)

143 2.1.2 Effect of time averaging sensors on source inference for a single source

144 Since we consider time averaging concentration samplers, we develop the time-averaged equation of **Eq. (1)**
145 over **an integration** time period τ :

146

$$147 \quad \overline{C(x)} = \overline{D(x)} \times \overline{S} + \overline{C_{bgd}} \quad (2)$$

148

149 where the overbars denote a time average over the period τ . Similarly as what is done in turbulent flux
 150 calculations, the first part of the right hand side of **Eq. (2)** is decomposed using the Reynolds decomposition of a
 151 random variable (Kaimal and Finnigan, 1994), giving:

152

$$153 \quad \overline{C(x)} = \overline{D(x)} \times \bar{S} + \overline{C_{bgd}} + \overline{D'(x)S'} \quad (3)$$

154

155 where $\overline{D'(x)S'}$ is the time covariance between $D(x,t)$ and $S(t)$. If the averaged background concentration $\overline{C_{bgd}}$ is
 156 a known quantity, **Eq. (3)** can be easily manipulated to give an estimation of the averaged source strength \bar{S} , the
 157 quantity we want to infer:

158

$$159 \quad \bar{S} = \frac{\overline{C(x)} - \overline{C_{bgd}}}{\overline{D(x)}} - \frac{\overline{D'(x)S'}}{\overline{D(x)}} \quad (4)$$

160

$$(I) \quad (II)$$

161 In the right hand side of **Eq. (4)**, (I) can be calculated from measured $\overline{C_{bgd}}$ and $\overline{C(x)}$ and $\overline{D(x)}$ which is itself
 162 calculated with dispersion models. On the contrary (II) is *a priori* unknown and depends on the correlation
 163 between the source strength and the transfer function $\overline{D'(x)S'}$. Hence, if (II) is neglected, the inferred source \bar{S} is
 164 biased. The relative bias of the method is then:

165

$$166 \quad \frac{\delta \bar{S}}{\bar{S}} = \frac{\overline{D'(x)S'}}{\overline{D(x)} \times \bar{S}} \quad (5)$$

167

168 Hence we show in **Eq. (5)** that time-averaging leads to a relative bias which can be quantified by the time
 169 covariance between the transfer function and the source strength. However this quantity is by nature unknown
 170 since the dynamics of $S(t)$ is unknown. Determining $\overline{D'(x)S'}$ requires knowledge of the source dynamics which
 171 can be obtained from measurements with a micrometeorological method. It can alternatively be approached by
 172 modelling using the state of the art of ammonia exchange processes as we do here.

173 Additionally to the bias, which is term (II) in **Eq. (4)**, evaluating term (I) is encompassed with errors related to
 174 the uncertainties in $\overline{C_{bgd}}$, $\overline{C(x)}$ and $\overline{D(x)}$. In particular, cases when $\overline{D(x)}$ is small may lead to large errors in
 175 inferring the source term S . This is linked to the conditioning of the inverse problem and is discussed in
 176 supplementary material S2.

177 2.1.3 Case of multiple sources and multiple concentration samplers with time averaging

178 If we generalise the approach to multiple sources and multiple receptors, then the transfer function becomes a
 179 matrix $D(x_i, S_j, t)$, which is the contribution of source S_j to concentration at target located at x_i . For reading
 180 purposes we simplify the matrix notation to D_{ij} . **Eq (3)** then becomes:

181

$$182 \quad \begin{bmatrix} \overline{C_1} \\ \vdots \\ \overline{C_M} \end{bmatrix} = \begin{bmatrix} D_{1,1} & \cdots & D_{1,M} \\ \vdots & \ddots & \vdots \\ D_{N,1} & \cdots & D_{N,M} \end{bmatrix} \times \begin{bmatrix} \overline{S_1} \\ \vdots \\ \overline{S_M} \end{bmatrix} + \overline{C_{bgd}} + \begin{bmatrix} D'_{1,1} & \cdots & D'_{1,M} \\ \vdots & \ddots & \vdots \\ D'_{N,1} & \cdots & D'_{N,M} \end{bmatrix} \times \begin{bmatrix} \overline{S'_1} \\ \vdots \\ \overline{S'_M} \end{bmatrix} \quad (6a)$$

183

184 Which in condensed notation gives:

185

$$\overline{C(x_i)} = \overline{D_{i,j}} \times \overline{S_j} + \overline{C_{bgd}} + \overline{D'_{i,j}} \times S'_j \quad (6b)$$

187

188 If the number of targets is equal to the number of sources, the problem can be solved by inversion of a linear
189 system. If the number of targets is larger than the number of sources, the problem is a multiple linear regression
190 type with unknowns $\overline{S_j}$ and $\overline{C_{bgd}}$. The third term on the right hand side of the **Eq. (6b)** is a bias which is *a priori*
191 unknown and which we will evaluate in this study.

192 2.1.4 Source inference methods

193 The inferred sources, $\overline{S_i^{inferred}}$, were derived from **Eqns. (3)** or **(6)** assuming the covariance term (last term on
194 right hand side) was null. The method used to infer the source was either a simple division (**Eq. (3)**) or an
195 optimisation of the linear system using the linear model function *lm* in R (package stats, R version 3.2.3), with
196 either $M = 1$ (single source) or $M = 9$ (multiple sources):

197

$$\begin{bmatrix} \overline{D_{1,1}} & \dots & \overline{D_{1,M}} \\ \vdots & \ddots & \vdots \\ \overline{D_{N,1}} & \dots & \overline{D_{N,M}} \end{bmatrix} \times \begin{bmatrix} \overline{S_1^{inferred}} \\ \vdots \\ \overline{S_M^{inferred}} \end{bmatrix} = \begin{bmatrix} \overline{C_1} \\ \vdots \\ \overline{C_N} \end{bmatrix} - \overline{C_{bgd}} \quad (7)$$

199

200 The bias δS_i was then evaluated as the difference between the inferred sources $\overline{S_i^{inferred}}$ and the modelled
201 sources $\overline{S_i^{obs}}$ averaged over each period:

202

$$\delta S_i = \overline{S_i^{inferred}} - \overline{S_i^{obs}} \quad (8)$$

204

205 As shown in **Eqns. (3)** and **(6)** the overall mean bias δS_i contains (i) a bias term due to the inference method
206 which is dependent mainly on the conditioning of the matrix D_{ij} (see supplementary material S2) and (ii) a bias
207 term which is intrinsically linked to the covariance between D_{ij} and S_j (**Eqns. 3** et **6**). Thus, with **Eq. (8)** we
208 evaluate the sum of the two biases without distinction. In order to infer the sources, the elements of the
209 dispersion matrix D_{ij} need to be determined. The next part details how these were estimated with a dispersion
210 model.

211 2.2 The dispersion model used for determining the transfer matrix D_{ij}

212 The elements of the transfer matrix $D_{ij} = D(x_i, S_j, t)$, **that is** by definition the concentration at location x_i and time
213 t generated by a source S_j of strength $S_j(t) = 1$, **were calculated using a dispersion model..** The FIDES-3D
214 model ("FIDES", Loubet et al., 2010), based on the analytical solution of the advection-diffusion equation of
215 Philip (1959) was used for that purpose. This model was first compared with a backward Lagrangian Stochastic
216 dispersion model (**bLS**, the "WindTrax" software, Thunder Beach Scientific, Nanaimo, Canada, Fleisch et al.,

217 | 1995), **and successively tuned to mimic the bLS**. The two models and how the FIDES model was tuned are
218 | briefly described hereafter and detailed in the supplementary material sections S3 and S4.

219 | The FIDES model is based on the Philip (1959) solution of the advection-diffusion equation, which assumes
220 | power law profiles for the wind speed $U(z)$ and the vertical diffusivity $K_z(z)$ **at height z** . This approach also
221 | assumes no chemical reactions in the atmosphere and spatial horizontal homogeneity of roughness length (z_0),
222 | wind speed (U), vertical and lateral diffusivity (**K_z and K_y**). The dispersion model is detailed in Huang (1979),
223 | and Loubet (2010). The details of the model and the way the transfer function $D(x_i, S_j, t)$ was estimated is
224 | detailed in the supplementary material S2.

225 | The Schmidt number which is the ratio of momentum to scalar vertical diffusivity $Sc = Km_z / K_z$ is key in
226 | dispersion modelling, as it determines the vertical diffusion rate of scalars. Wilson (2015) demonstrated that bLS
227 | and dispersion models like FIDES give different values of Sc by constitution. In order to assure consistency of
228 | the **Philip** (1959) approach with bLS models, considered as references in dispersion modelling, we chose to tune
229 | the Philip (1959) model to get the same Sc number as in WindTrax as described by Flesch et al. (1995). The
230 | details are given in supplementary material S4. The comparison showed that the tuned FIDES model gives very
231 | similar concentrations to WindTrax at measurement heights lower than 2 m above the source, although slightly
232 | overestimated under stable and neutral conditions and slightly underestimated under unstable conditions. The
233 | correlation between the two models is however very high ($R^2 \geq \sim 0.96$) meaning that using the tuned FIDES
234 | model to characterise source inference performance, will lead to results **comparable** to WindTrax. Moreover
235 | since in this study the same model is used for predicting and for inferring the fluxes the results are self-
236 | consistent.

237 | **2.3 Ammonia sources from simple SVAT modelling and prescribed emission potentials**

238 | In order to evaluate the bias introduced by time averaging the concentrations when inferring single or multiple
239 | sources (third term in **Eqns. 3** and **6**), we generated NH_3 emission patterns mimicking the behaviour of real
240 | sources as closely as possible. In that prospect, we used the SurfAtm- NH_3 model developed by Personne et al.
241 | (2009) for two purposes: (i) evaluating the turbulence parameters (the friction velocity u_* , and the Monin
242 | Obukhov length L) from the meteorological datasets to parameterise the dispersion models, and (ii) providing the
243 | surface temperature $T(z_0)$ and the surface resistances in order to calculate ammonia emission patterns.

244 | The SurfAtm- NH_3 model is a one-dimensional, bi-directional surface-vegetation-atmosphere-transfer (SVAT)
245 | model, which simulates the latent (LE) and sensible (H) heat fluxes, as well as the NH_3 fluxes between the
246 | biogenic surfaces and the atmosphere. It is a resistance analogue model separately treating the vegetation layer
247 | and the soil layer, and coupling a slightly modified (Choudhury and Monteith, 1988) model of energy balance
248 | and the two-layer bi-directional NH_3 exchange model of (Nemitz et al., 2000) with a water balance model.
249 | Unless otherwise stated, the surface was considered a bare soil with $z_0 = 5$ mm, **displacement height (d)** = 0 m,
250 | and **leaf area index (LAI)** = 0.

251 | The ammonia emission patterns were modelled using the resistance approach and assuming atmospheric
252 | concentration was zero, which is a reasonable assumption following nitrogen application and leads to patterns
253 | mimicking reality, which is what we are seeking here:

$$254 | \quad \quad \quad 255 | \quad F = \frac{C_{p\text{ground}}}{R_a(z_{ref}) + R_{b\text{NH}_3}} \quad (9)$$

256

257 | Where $R_a(z_{ref})$ is the aerodynamic resistance at the reference height $z_{ref} = 3.17$ m, and R_{bNH_3} is the soil
258 | boundary layer resistance for ammonia as described in Personne et al. (2009). The ground surface compensation
259 | point concentration ($C_{pground}$) was expressed as a function of Γ , the ratio of NH_4^+ to H^+ **concentrations** in the
260 | soil **liquid phase** at the surface, as in Loubet et al. (2012):

261

$$262 | \quad C_{pground} = K_h\{T(z_0)\} \times K_d\{T(z_0)\} \times \Gamma = \Gamma \times 10^{-3.4362+0.0508 T(z_0)} \quad (10)$$

263

264 | where K_h and K_d are the Henry and the dissociation constant for NH_3 **respectively**, and $T(z_0)$ is the soil surface
265 | temperature. Since we wanted to evaluate the correlation between the transfer function D_{ij} and the source
266 | strength S_j , which is the bias in the inference problem (**Eq. 6**), the NH_3 volatilisation was modelled as to
267 | reproduce the variety of existing kinetics of NH_3 emissions from fields. In that prospect, three Γ patterns were
268 | simulated:

269

1. a constant $\Gamma = \Gamma_0$, which would mimic background NH_3 emissions from soils;

270

2. an exponentially decreasing $\Gamma = \Gamma_0 \exp(-4.6 t / \tau_0)$, which best represents NH_3 emissions following
271 | slurry application ;

272

3. a Gaussian $\Gamma = N(\Gamma_0, \sigma_\Gamma)$, which would represent the typical NH_3 emissions following urea application.

273

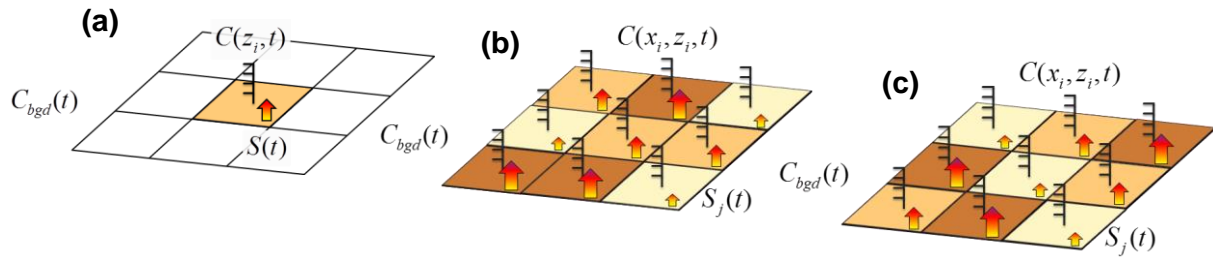
Here Γ_0 is the maximum Γ during the period, t is the time in days, τ_0 is the duration of the emission in days. The
274 | factor 4.6 was chosen so that when $t = \tau_0$, Γ goes down to 1% of Γ_0 . The duration of the emissions was chosen to
275 | be four weeks, $\tau_0 = 28$ days. **The time scale of the exponential decrease we used here was around 6 days,**
276 | **which is twice as large as the one reported by Massad et al. (2010) for slurry application (2.9 days).** While
277 | these Γ patterns gave the weekly trend of NH_3 emissions, the daily patterns were produced by the
278 | thermodynamical and turbulence drivers of NH_3 emissions which were explicitly taken into account through the
279 | compensation point (**Eq. 10**). To facilitate understanding, in most of the manuscript only the constant Γ was
280 | considered, and the effect of modifying the source strength was evaluated in a sensitivity study.

281 | **2.4 Spatial set up of the sources, concentration sensors**

282

The sources (plots) were considered as squares with width x_{plot} and aligned south-north. Two configurations were
283 | considered: (1) a single source configuration and (2) a multiple-sources configuration which mimics typical
284 | agronomic trials with 9 sources (plots) placed next to each other, with three treatments times three repetitions.
285 | Each treatment was assigned a value of Γ_0 different from the others, while the three repetitions of the same
286 | treatment were assigned the same value of Γ . The concentration sensors (receptors) locations, x_i , were set in the
287 | middle of each plot, at several heights z_i . (**Figure 1**).

288



289

290 **Figure 1. General scheme of the source receptor locations for (a) a single source, and (b) multiple-sources. (c)**
 291 **“optimum” plot layout used for the multiple-source configuration.**

292 A number of plot sizes ($x_{\text{plot}} = 25, 50, 100$ and 200 m on the side), and receptor heights ($z_i = 0.25, 0.5, 1$ and 2
 293 m), were tested successively. Several source strengths and dynamics were also tested: Γ was first considered
 294 constant with time (pattern 1) in all the plots, and the Γ_0 of each of the three treatments were either chosen to be
 295 significantly different in strength ($10^4, 10^5, 10^6$), or of the same order of magnitude (1000, 2000, 4000). Then the
 296 three Γ patterns (“constant”, “exponential” and “Gaussian”) were randomly assigned to the treatments for each
 297 simulation period. The ammonia background concentration, C_{bgd} , was considered constant and equal to 1 ppb
 298 except when studying the sensitivity of the inference method to the background concentration, where it was set
 299 as unknown. Throughout this study, an “optimum” block configuration was considered (shown in **Figure 1c**),
 300 which avoided trivial configurations like aligned blocks and maximised the mean distance between blocks **as in**
 301 **a Latin-square design.**

302 2.5 Simulation details

303 2.5.1 Meteorological data and fertiliser application periods

304 A range of meteorological conditions were simulated based on the half-hourly meteorological data of the FR-Gri
 305 ICOS site in 2008. In total 13 periods of 28 days were considered which spanned the whole year except the last
 306 two days of the year. Each period consisted of 1344 half-hourly data.

307 2.5.2 Concentration sensor integration periods

308 In order to evaluate the influence of the concentration averaging period on the source inference, several
 309 integration periods τ were tested: 0.5h (no integration), 3h, 6h, 12h, 24h, 48h, 168h (7 days). In practice the
 310 concentrations were computed at each sensor location using **Eq. (6)** over 0.5h: at that **time scale, which**
 311 **corresponds to the spectral-gap**, the covariance term is assumed to be negligible (Van der Hoven, 1957). Then
 312 the averaged concentrations were computed for all integration periods.

313 2.5.3 Sensitivity to inferential methods scenarios

314 Several **scenarios** were considered and summarized in Table 1:

- 315 1) the background concentration $\overline{C_{bgd}}$ was either supposed known and fixed to the prescribed values (**C1-**
 316 **C4**) or was inferred (**C5-C7**);
- 317 2) the three repetitions of each treatment were either supposed to have the same source strength (**C2, C4,**
 318 **C5, C6**) or they were inferred independently (**C1, C3, C7**). In **C2, C4, C5** and **C6**, $S_i = S_m$ for all i and
 319 m belonging to the same treatment. In practice a new dispersion matrix was calculated by averaging

320 together all columns belonging to the same treatment (matrix dimension $N \times 3$). Three strength values
 321 of S were inferred to be tested;

322 3) either one concentration sensor at each source location (z_i) was considered (**C1, C2, C5**) or two sensors
 323 positioned at two heights were considered (**C3, C4, C6, C7**). All the measurement heights and their
 324 combinations were considered.

325

326 **Table 1. Scenarios tested for inferring the sources and background concentration.**

Strategy	Number of sensors	Plots [#] have same source strength in a given treatment	Background concentration	Note
C1	1	No	known	Each block is considered independently
C2	1	Yes	known	Each block is considered equal
C3	2	No	known	Identical to C1 except for the number of sensors
C4	2	Yes	known	Identical to C2 except for the number of sensors
C5	1	Yes	unknown	Identical to C2 except for the background concentration estimation
C6	2	Yes	unknown	Identical to C4 except for the background concentration estimation
C7	2	No	unknown	Identical to C3 except for the background concentration estimation

327 # **Each** treatment **have 3 plots** (repetitions).

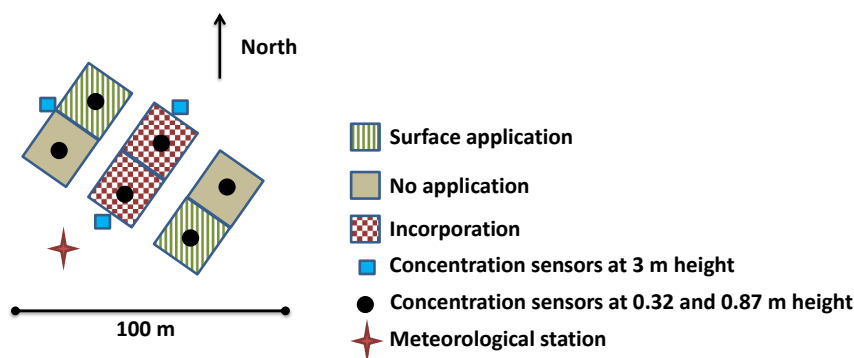
328 2.6 Statistical indicators

329 For each run the mean bias (**BIAS**) and the normalised mean bias (**NBIAS**), were calculated as: $BIAS_i =$
 330 $\frac{1}{N_\tau} \sum_\tau \delta cum S_i$, $NBIAS_i = BIAS_i / \left(\frac{1}{N_\tau} \sum_\tau cum S_i^{obs} \right)$, where N_τ is the number of the time averaged samples over
 331 each 28-day period and $cum S_i$ and $cum S_i^{obs}$ are the **inferred and observed** cumulated fluxes over the same
 332 period. The medians and interquartile of these statistical indicators were then calculated over the 13 periods of
 333 28-days for 2008.

334 2.7 Real experimental test case

335 In order to evaluate the feasibility of the method we applied it to a real test case (**Figure 2**). The trial was located
 336 at La Chapelle Saint-Sauveur in France (47°26'44.1"N, 0°58'50.7"W) and performed from 5th April to 26th April
 337 2011. Soil texture **was loamy with a** pH in water **of** 6.2 and **a** bulk density **of** 1.4 t m^{-3} in the first 15 cm. The
 338 experimental unit **was composed by** 6 squared sub-plots of 20 m **wide** with 2 repetitions of 3 treatments: (1)
 339 surface application of cattle slurry, (2) surface application and incorporation of the same slurry and (3) no
 340 application. **Slurry** pH **was** 7.5 **with** dry matter (DM) **content** of 6.05%, C:N ratio of 10.4 and contained
 341 38.4 g N kg^{-1} (DM) as total nitrogen and $13.2 \text{ g N-NH}_4 \text{ kg}^{-1}$ (DM) as ammoniacal nitrogen. Slurry was applied
 342 on 5th April 2011 at a rate of $49 \text{ m}^3 \text{ ha}^{-1}$ which led to **119** kg N ha^{-1} and **41** $\text{kg N-NH}_4 \text{ ha}^{-1}$. The application was
 343 identical between the **two** repetitions with a small standard deviation ($< 0.2 \text{ kg N ha}^{-1}$). The incorporation was
 344 performed in two sub-plots one hour after the end of the slurry spreading with a disc harrower at a depth of
 345 0.10 m. The soil humidity between 0 and 5 cm depth was homogeneous over the blocks and decreased from
 346 $20 \pm 1\%$ to $17 \pm 1\%$ w/w between the start and the end of the experiment. Meteorological data were measured **at**
 347 **less than 50 m from the central plots** (**Figure 2**). Air temperature, relative humidity, global solar radiation,
 348 wind velocity and direction were recorded every 30 minutes at 2 m height. The **turbulence** parameters (u_s and
 349 L), **input of the dispersion models**, were evaluated with a simple energy balance model of Holtslag and Van
 350 Ulden (1983) assuming a Bowen ratio of 0.5 and a deep soil temperature equal the averaged ambient
 351 temperature. Ammonia concentration was measured with diffusive samplers (ALPHA), (Sutton et al., 2001;

352 Tang et al., 2001; Tang et al., 2009), which were placed at the centre of each sub-plot at two heights (0.32 and
 353 0.87 m from the ground) as well as next to the assay at three location (5 m away from the plots) at 3 m height.
 354 The ALPHA samplers were set in place just after slurry application and incorporation (between 14:20 and 14:50)
 355 and left exposed subsequently for **3h, 22h, 23h, 23h, 71h** (3 days) and **359h** (15 days) hence spanning 21 days.
 356 The diffusive samplers were prepared prior to the experiment, stored at 4°C in a refrigerator and analysed by
 357 colorimetry. Since no background concentrations were measured at a reasonable distance from the field, the
 358 background concentration was assumed as the minimum over the whole period of the concentrations measured
 359 on the 3 m height masts.

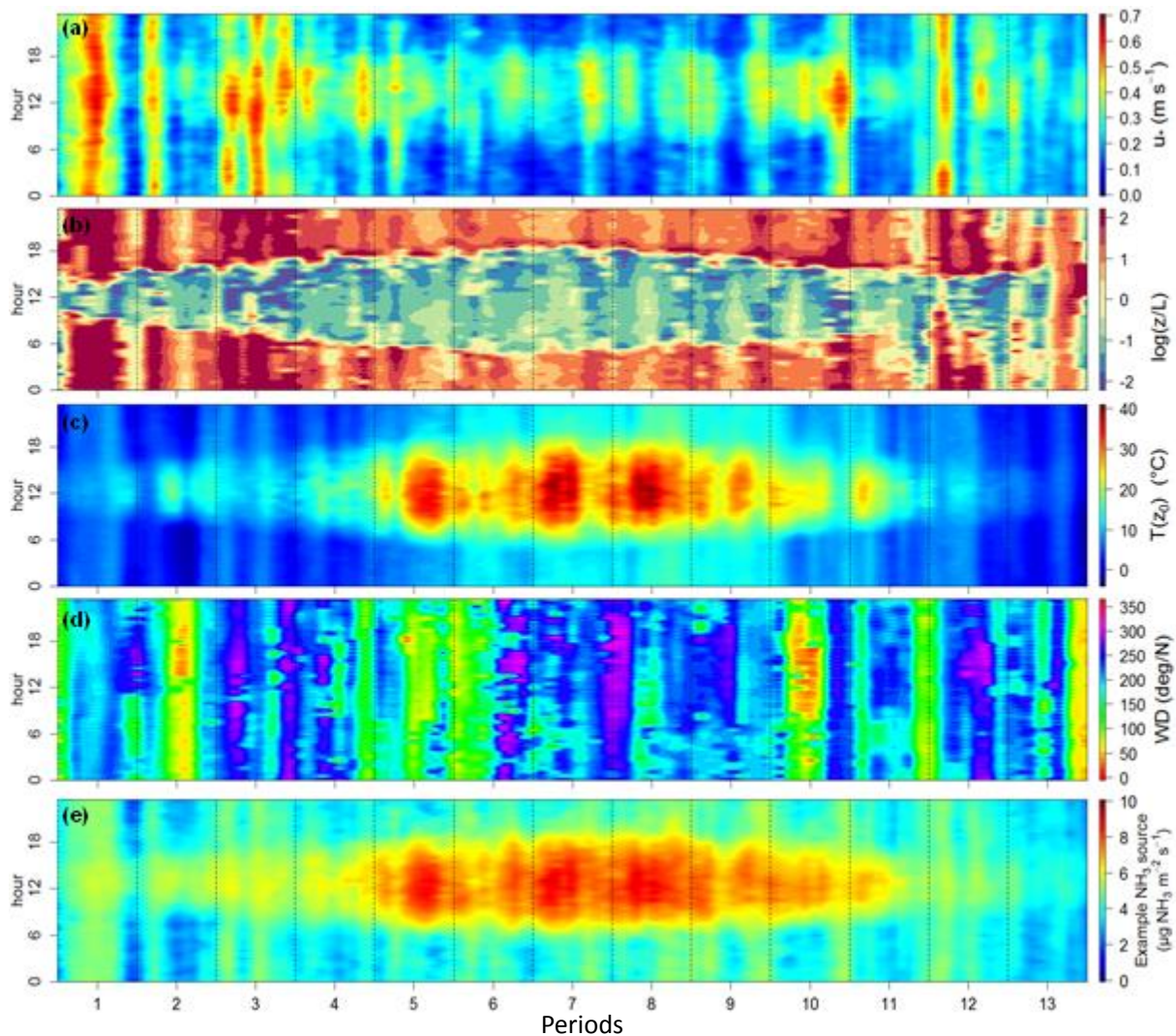


361 **Figure 2. Scheme of the real experimental test case performed on 6 sub-plots with three treatments and two**
 362 **repetitions. Cattle slurry was either applied on the surface or incorporated. The concentration sensor and**
 363 **meteorological station locations are shown on the scheme.**

364 3 Results and discussion

365 3.1 Meteorological data range and simulated ammonia sources

366 The meteorological conditions over the 13 periods represented a good sample of temperate climate conditions.
 367 **The friction velocity u_* varied between 0.024 and 1.181 m s⁻¹**, and the stability parameter **z/L at 1m height**
 368 **varied between -49 and 21 (Figure 3)**. It is noticeable that u_* showed greater variability during the winter than
 369 during the summer, while it was the opposite for z/L . The surface temperature also showed a structure varying
 370 between periods, with a larger temperature range during the summer (from 5.7 to 50.4°C) than during the winter
 371 (from -5.2 to 22.9°C). This surface temperature variability is an essential feature to representing real case
 372 ammonia sources (Sutton et al., 2009), which shows a variability reflecting both the surface temperature and the
 373 resistances variations (Eqns. 9 and 10).

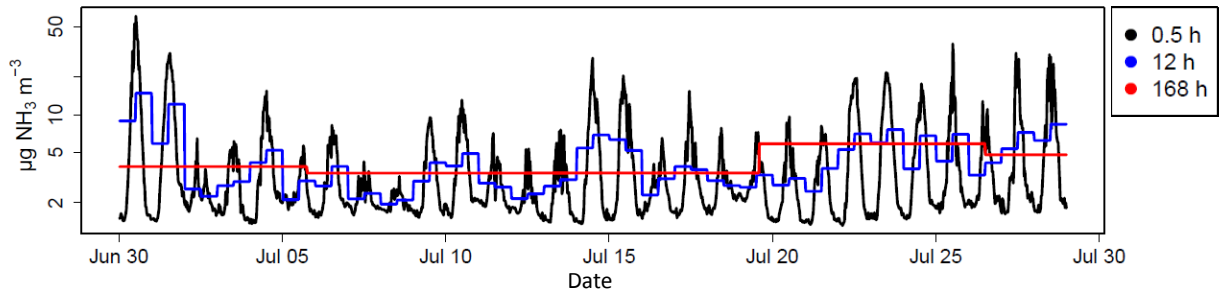


374
 375 **Figure 3. Footprints of measured u_* (a), z/L at 1 m height (b), $T(z_0)$ (c), and wind direction (d) for the hour of the day**
 376 **and the 13 considered periods over year 2008 in the FR-GRI ICOS site. The modelled ammonia source is also**
 377 **reported (e) according to Eqns. (9) and (10) over the same period with an emission potential $\Gamma = 10000$.**

378

379 3.2 Example ammonia concentration dynamics modelled with the tuned FIDES model

380 The modelled ammonia concentrations reproduced typical patterns measured above field following nitrogen
 381 application well, with maximum concentrations during the day and minimum concentrations at night (**Figure 4**).
 382 These patterns are a consequence of daily variations of the sources driven by surface temperature combined with
 383 variations in the aerodynamic transfer function D_{ij} , which behaves similarly as a transfer resistance (see
 384 supplementary material S1). The integration periods are also shown in **Figure 4**, which illustrates the progressive
 385 loss of information of the pattern structure with integration periods. Particularly, it can be seen that the day-to-
 386 night variation is captured up to an integration period of 6h. Moreover, it should be noted that averaging also
 387 means overestimating lower concentrations and underestimating higher concentrations.



388
389

390 **Figure 4. Example modelled concentration pattern at 1 m above a single 50 m width source for several averaging**
391 **periods (0.5h, 12h and 168h) for the month of July 2008. The source Γ was set to 10^5 . The y-axis is log scaled.**

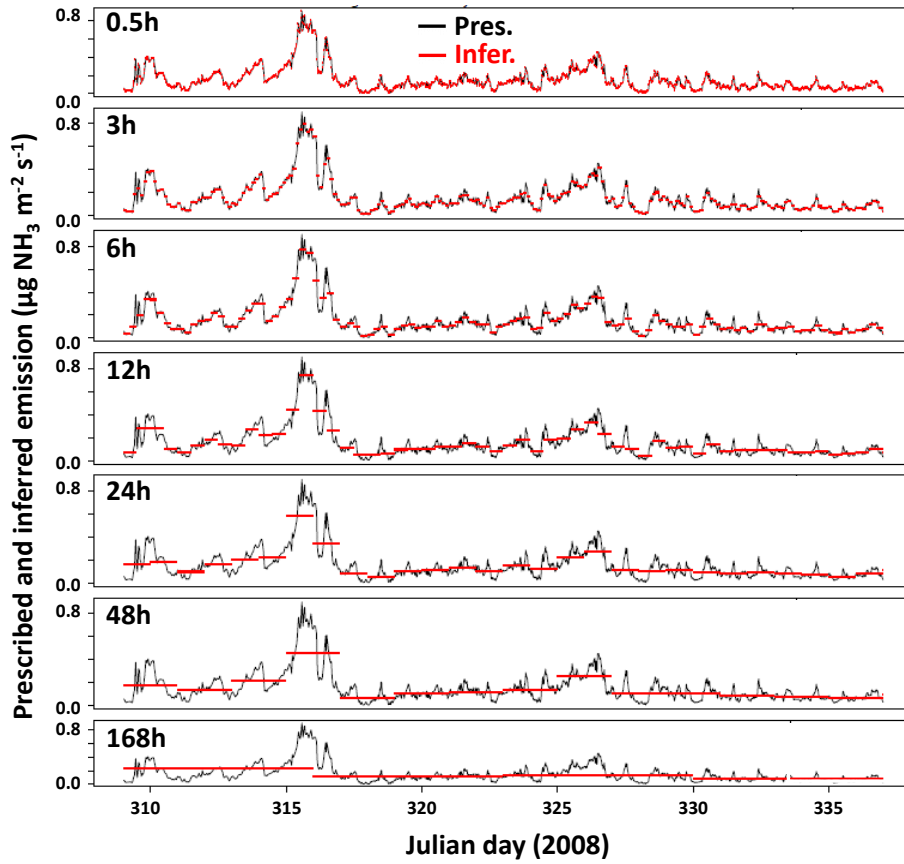
392

393 3.3 Evaluation of the inference method for a single source and a single sensor

394 At first we evaluate the bias of the inference method for the simpler case of a single source and a single sensor
395 placed in the centre of the source field at several heights, assuming we know the background concentration
396 (strategy C1; **Figure 1a.**). This case has the advantage of having a condition number equal to 1 (**Supplementary**
397 **material section S2 and Eq. S1**) and a bias δS which is well defined and equal to $-\overline{[D]}^{-1} \times \overline{[D'S']}$ (**Eq. (8)**).
398 This section hence **focuses** on evaluating the influence of sensor height, time integration, and source dimension
399 on the bias without dealing with the complexity of the interactions between multiple fields.

400 3.3.1 Example inferred source dynamics

401 **Figure 5** reports an example source inference, which shows the progressive smoothing of the source with
402 integration period. We first see that the source strength corresponding to $\Gamma = 10^5$ leads to ammonia emissions
403 ranging from 0 to $\sim 1 \mu\text{g NH}_3 \text{ m}^{-2} \text{ s}^{-1}$ in the winter, which corresponds to $0.71 \text{ kg N ha}^{-1} \text{ day}^{-1}$. Over the entire
404 year, the maximum emission occurs during the hottest days and reaches up to $7.1 \text{ kg N ha}^{-1} \text{ day}^{-1}$. Regarding the
405 inference method, it can be seen in that example that up to 24 hours the variability in emissions over the period is
406 captured quite well.



407

408 **Figure 5. Example source inference for a 25 m width square field and a concentration sensor placed at 0.5 m above**
 409 **ground. Here $\Gamma = 10^5$ and is set to constant (pattern 1). The 7 integration periods are shown: 0.5h to 168h. The x-axis**
 410 **shows the day of year and corresponds to a span over November. The prescribed source is in black (Obs.) and the**
 411 **inferred one in red (Pred.)**

412

413 3.3.2 Effect of target height, source dimension and integration period on the bias δS for a single source

414 In this simpler case shown in **Figure 6**, the fractional bias of the inferred emission is mostly negative for the
 415 combination where the ratio sensor height / plot dimension is small and integration times are larger than 6h.

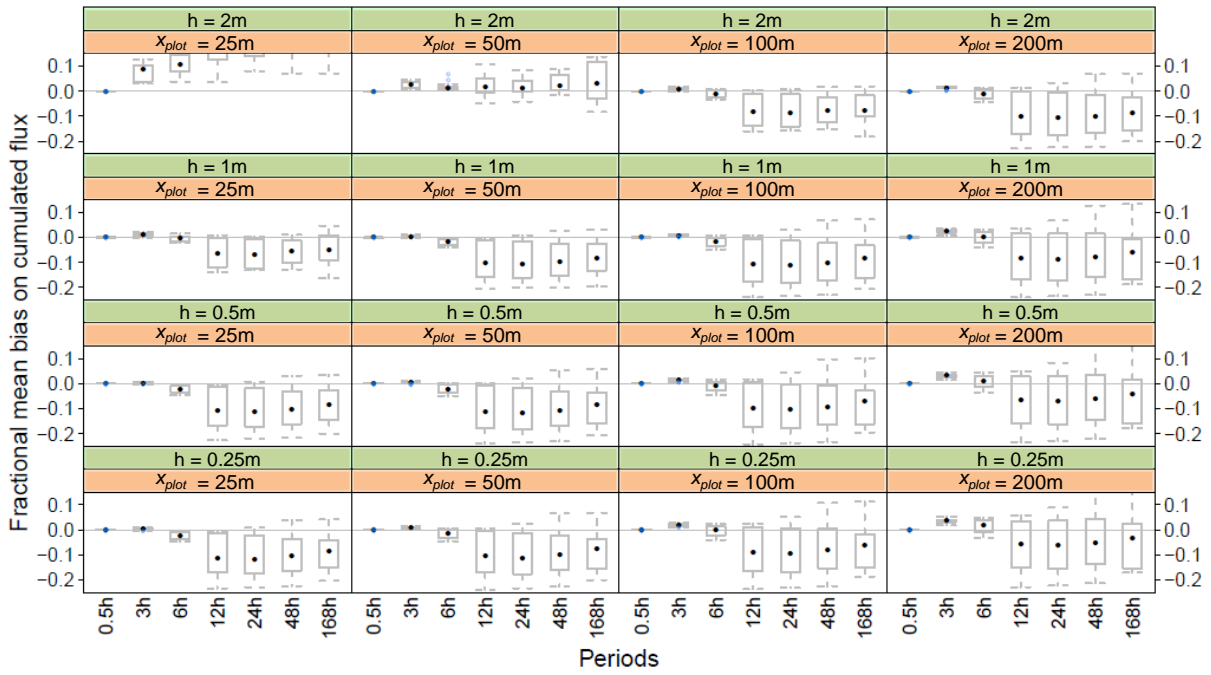
416 According to **Eq. (5)**, this means that the covariance term $\overline{D'S}$ is negative for these conditions, meaning that any
 417 increase in source strength S at a time t is correlated with a decrease of the transfer function $D(t)$ and vice versa.

418 This is expected as $S(t)$ increases with the surface temperature (**Eq. (10)**) and is proportional to $[R_a(z_{ref}) +$
 419 $R_{bNH_3}]^{-1}$ (**Eq. (9)**), while $D(t)$ is proportional to the aerodynamic resistance $R_a(z_{ref})$, as shown in supplementary

420 material S1. Hence, over daily periods, S and D are negatively correlated: S increases during the day and
 421 decreases at night (due to temperature and wind speed daily patterns), while D decreases during the day and
 422 increases at night (mainly due to wind speed patterns). This is expected to be a general feature for NH_3 surface
 423 fluxes as the daily variability reproduced by the model used in this study is representative of most situations
 424 from mineral and organic fertilisation, to urine patches or seabird colonies (Ferrara et al., 2014; Flechard et al.,
 425 2013; Milford et al., 2001; Moring et al., 2016; Personne et al., 2015; Riddick et al., 2014; Sutton et al., 2013).

426 The median bias δS_i tends to increase in magnitude with the sensor height for large fields ($x_{plot}=100$ and 200 m)
 427 whilst decreases for smaller fields ($x_{plot} = 25$ and 50) when sensor height gets close to the field boundary layer

428 height. Furthermore, δS_i becomes positive and very large when sensors get above the field boundary layer
 429 height (**Figure 6**). For large fields, the increase of the magnitude of the bias with lower sensor height is expected
 430 as D decreases with height in absolute value. For small fields, the decrease of the bias corresponds to a loss of
 431 information as D gets close to zero when the sensor gets closer to the field boundary layer height. For heights
 432 above this limit, we observe a change in sign of the bias which can be explained by the fact that the sensor
 433 concentration footprint is not in the source during stable conditions (at night) while it is in the source under
 434 unstable conditions during the day. The inference method will hence not work if at least one sensor is not below
 435 the plot boundary layer height.



436 **Figure 6. Fractional bias of inferred cumulated ammonia emission for a single squared field of side (x_{plot}) 25, 50, 100**
 437 **and 200 m and sensors heights (h) 0.25, 0.5, 1 and 2 m, as a function of sensors integrating periods. The points show**
 438 **the median, the boxes the interquartile and the whiskers the maximum and minimum over the 13 application periods.**
 439

440
 441 We also notice that for integration periods **equal or** below 3h, the fractional bias is slightly positive, which can
 442 be explained by the positive correlation between S and D at small time scales. This is because of the influence of
 443 u_* on $T(z_0)$: for a given solar radiation and air temperature over small time scales ($< 3h$), an increase in u_* leads
 444 to a decrease in $T(z_0)$, which leads to an exponential increase of the surface compensation point according to **Eq.**
 445 **(10)**. However, at the same time, $R_a(z)^{-1}$ decreases, but linearly with u_* . The resulting ammonia emission
 446 calculated with **Eq. (9)** nevertheless increases because the exponential effect of temperature overcomes the linear
 447 effect of the exchange velocity (data not shown). This effect is more visible for large fields than small fields
 448 because over small fields an additional effect is that when u_* decreases, the footprint increases and the source
 449 “seen” by the targets hence decreases because it incorporates a fraction of zero emission sources.

450 Overall, the median fractional bias for weekly integrated emissions over a 25 m field and sensor heights below
 451 0.5 m was overall -8% with an interquartile (-14% to -2%). We can conclude that the bias of the NH_3 emissions
 452 is reproducible within $\pm 6\%$. We can also conclude that it would be better to place the concentration sensor at a
 453 low height to minimise the bias of the method.

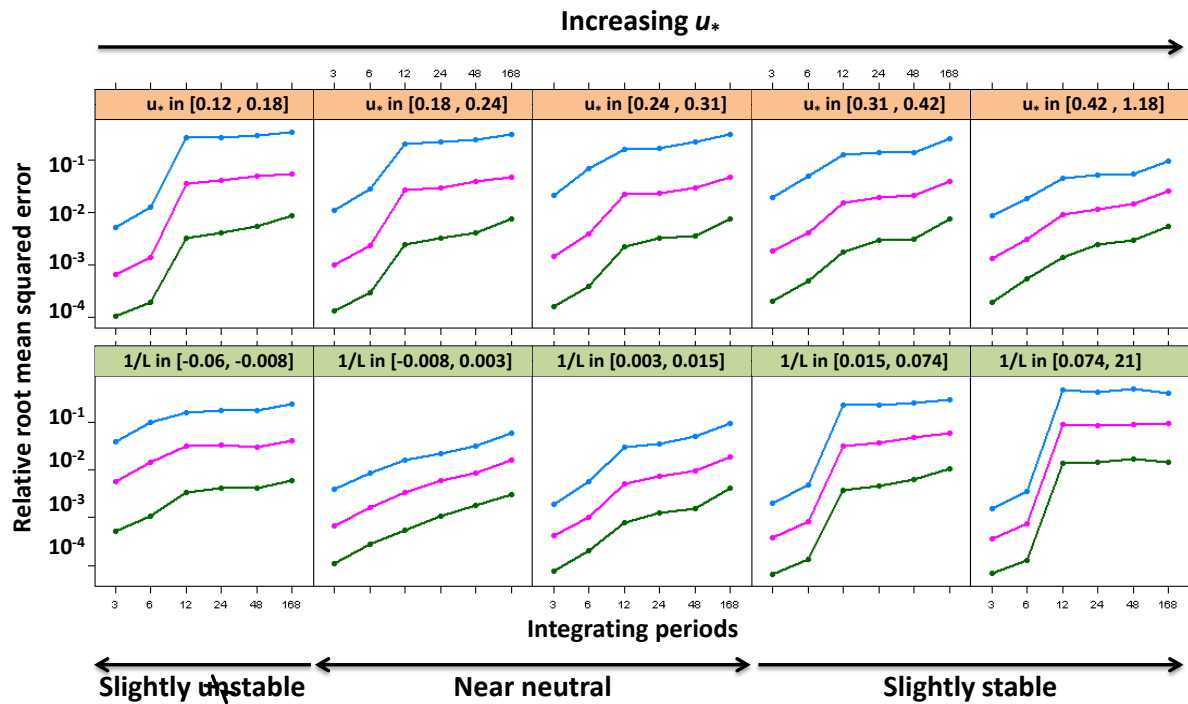
454

455

456 3.3.3 Effect of surface boundary layer turbulence on the inference method for a single source

457 The inference method depends on the turbulence at the site and especially on the main drivers of the dispersion
458 which are the friction velocity and the stability regime. Indeed **Figure 7** shows that the relative root mean square
459 residual of the inferred source (RRMSR) decreases with increasing u_* at long integration periods and is larger in
460 slightly stable than near-neutral or slightly unstable conditions. **Figure 7** also shows that the under stable
461 conditions or low u_* the RRMSR increases by more than an order of magnitude (up to 50%) when integration
462 periods increase from **6h** to **12h**, which catches most of the source variance. We also see that under near-neutral
463 or high u_* conditions, the 3rd quartile of the RRMSR remains below 10% for all integration periods. Finally, we
464 also see that the larger 3rd quartiles at short integration periods are obtained with intermediate u_* values or
465 slightly unstable conditions. A similar response of the bias to u_* and $1/L$ was reported by Figure 6 in (Flesch et
466 al., 2004) and Figure 3 in Gao et al. (2009) in controlled source experiments. While Gao et al. (2009) attributed
467 the bias of the inference method to parameterisation of the stability dependence of the turbulent parameters (z/L),
468 in this study this cannot happen since we use the same parameterisation for prescribing the concentration and
469 inferring it. In our case, the interpretation is to be linked with **Eq. (5)**: the smaller u_* or the most stable
470 conditions also correspond to the larger time-derivatives of source strength (driven by surface temperature and
471 surface exchange resistances) as well as the larger time-derivatives of transfer function D . We hence expect that
472 under such conditions, the covariance between the transfer function and the source strength will be larger than
473 under near-neutral conditions. In a more heuristic view, under low turbulence, large time-derivatives of
474 concentrations are expected above a source due to low mixing (small changes in mixing lead to large variations
475 in concentrations).

476 We conclude that the inference method with a long integration period will lead to very moderate biases for
477 locations with near-neutral conditions and high wind speed, but may lead to much larger bias under stable
478 conditions and low wind speed as soon as the integration period gets up to **12h**.

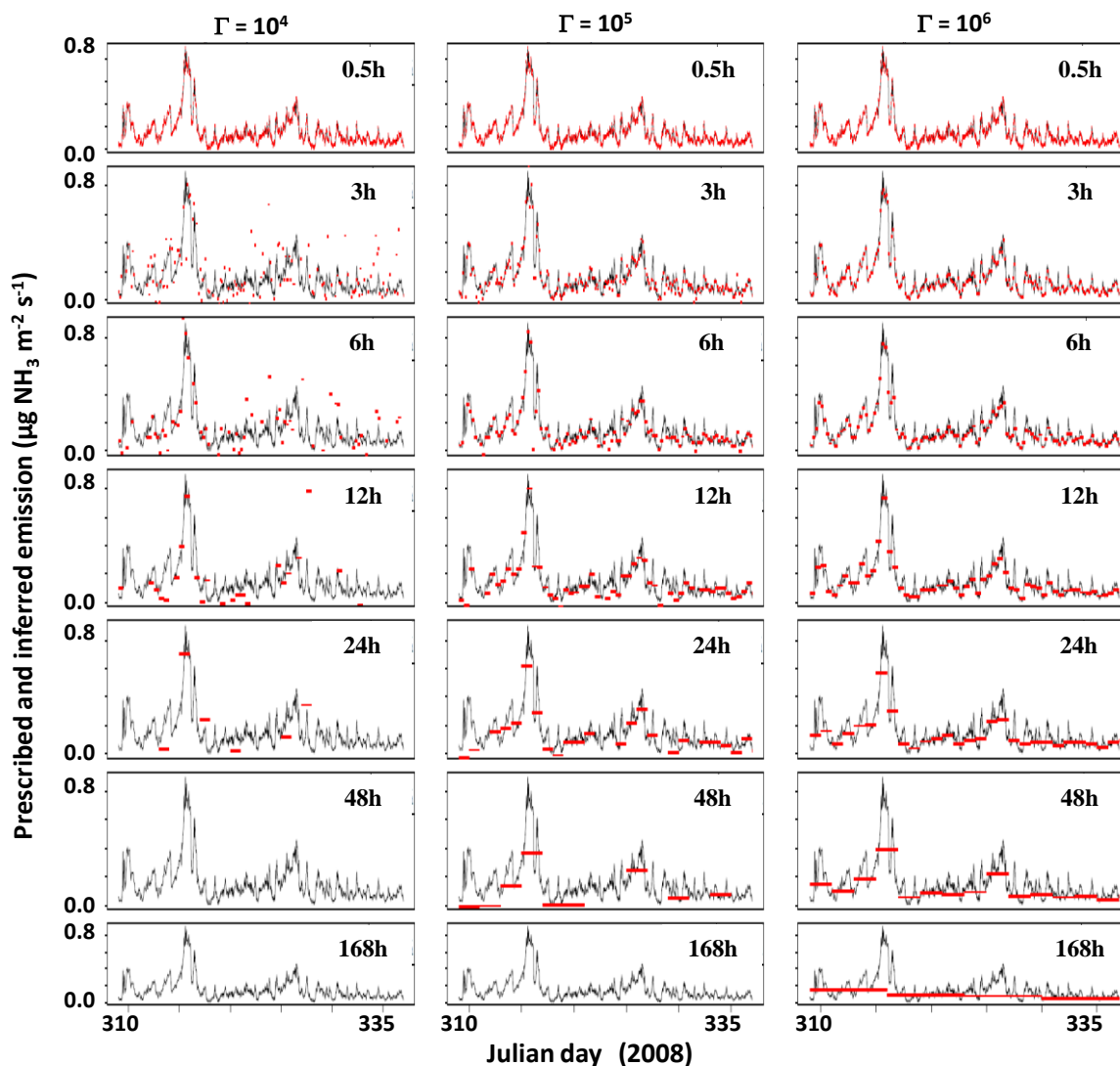


479
 480 **Figure 7.** Relative root mean squared error as a function of integration period for stability factor and friction velocity
 481 classes for a single 25 m side field. Medians and quartiles are given for equally sized bins of u_* and $1/L$ and for the
 482 lowest sensor height (0.25 m). The blue, pink and green curves are the 3rd, 2nd and 1st quartiles, respectively.

483

484 3.4 Multiple source case

485 In contrast to the single source case, with multiple sources (see **Figure 1b**) the inference method leads to biases
 486 at small integration times as can be seen in the example reported in **Figure 8**. In that specific case, the emissions
 487 of treatments-2 ($\Gamma = 10^5$) and 3 ($\Gamma = 10^6$) are 10 times and 100 times larger than that of treatment-1 ($\Gamma = 10^4$),
 488 respectively. This leads to concentrations over plots of treatment-1 (and to a lesser extent over those of
 489 treatment-2) being highly correlated to emissions from plots of treatment-3 (and hence less with sub-plots of
 490 treatment-1). As a result, inferring emissions of plots of treatment 1 becomes harder as soon as averaging periods
 491 become larger or equal to 3h. This can be viewed as a progressive loss of information of the treatment-1
 492 contribution to concentrations due to the overweighing contribution of treatment 3 plots. However, we also see
 493 that treatments 2 and 3 seem quite correctly inferred for integration times smaller than 48h.



494

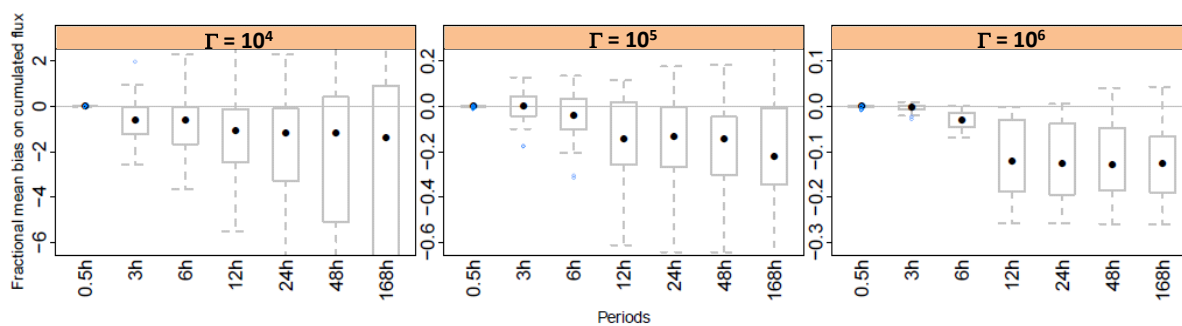
495 **Figure 8. Example result of multiple plot case inference. Black curves: observations; red dots: inferred sources. Left:**
 496 **treatment-1, $\Gamma = 10^4$. Middle: treatment-2, $\Gamma = 10^5$. Right: treatment-3, $\Gamma = 10^6$.** Missing red dots are out of the y-scale
 497 boundaries. Example plots from treatments 1, 2 and 3 are shown from left to right. The period is the same as in
 498 Figure 7 (November 2008 for the FR-Gri ICOS site), and emissions are up to 1, 10 and 100 $\mu\text{g NH}_3 \text{ m}^{-2} \text{ s}^{-1}$, for the
 499 three emission potentials. Strategy C7 with target heights 0.25 and 2 m, and source width 25 m on a side.

500

501 In the following we will first evaluate the influence of the length of integration periods, sensor heights and plots
 502 dimensions on the fractional biases made when inferring the source. Each factor will be evaluated independently
 503 of the others in order to understand the processes behind it. For these evaluations background concentration was
 504 kept constant at $1 \mu\text{g NH}_3 \text{ m}^{-3}$. Strategy C1 was used except when testing sensor heights for which strategy C3,
 505 which uses two targets, was also used. These two strategies assume that the background concentration is known
 506 which avoids any compensating effects between source and background concentration inferences. Then the
 507 sensitivity of the methodology to the (i) emission ratios between two of the three treatments and (ii) the
 508 variability in the background concentration were evaluated. Finally, seven inversion strategies were compared to
 509 determine which was the most robust (**Table 1**).

510 3.4.1 Effect of integration periods on the bias

511 We first consider strategy C1, which is the simplest configuration, in which plots are independent, background
512 concentration is known and one target is used above each plot. **Figure 9** shows that for the given treatment range
513 (~ 1 - 10 - $100 \mu\text{g NH}_3 \text{ m}^{-2} \text{ s}^{-1}$), the fractional mean bias is lower than 0.2 in magnitude for the treatment emitting
514 the most (treatment 3, $\Gamma = 10^6$), lower than 0.4 for the intermediate treatment (treatment-2, $\Gamma = 10^5$) and up to 8
515 for the treatment emitting the least (treatment-1, $\Gamma = 10^5$); here we considered the 0.25-0.75 quantiles. The bias
516 of the highest treatment (treatment -3) actually behaves similarly to a single source case (**Figure 6**), with a
517 median bias around 10% for 48h integration periods. This is expected because treatment-1 and treatment-2 have
518 much smaller emission strength and hence little influence on the concentration above the treatment-3 plots,
519 which therefore behaves in a similar manner to a single source. As a consequence, this bias in treatment-3 is
520 mainly due to the anti-correlation between D and S which increases with integration periods. The fractional
521 **mean** bias is very large for treatment-1 even for small integration periods. The bias can either be positive or
522 negative showing that this method does not allow for a correct estimation of the smallest sources.

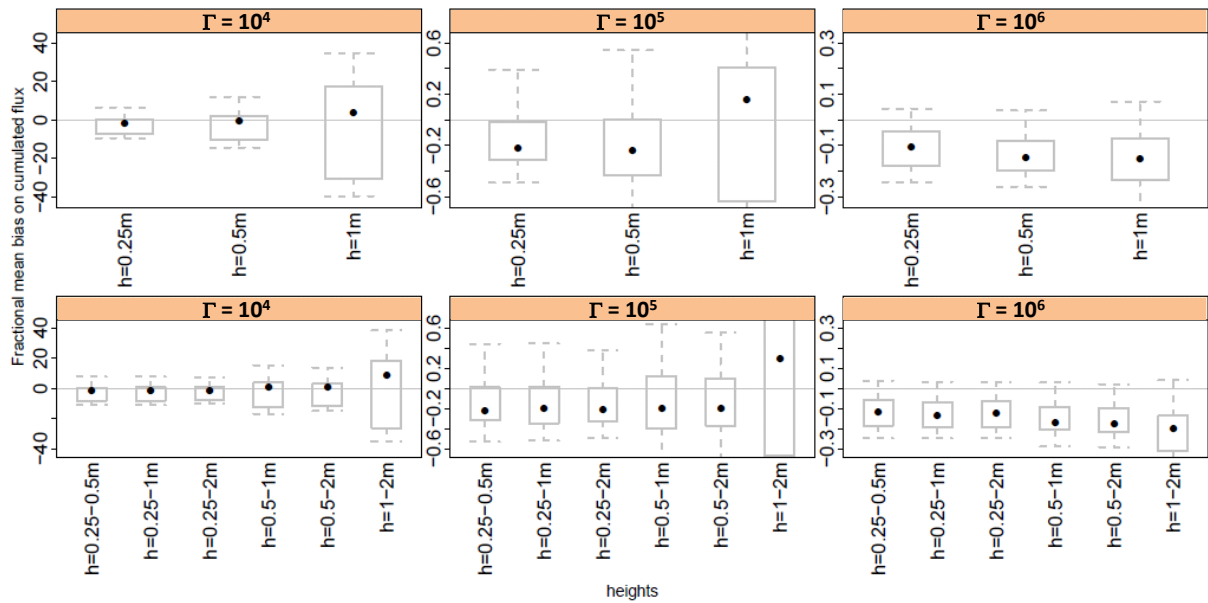


523 **Figure 9. Effect of integration period on source inference in a multiple-plot setup. The fractional mean bias of the**
524 **source is shown for each treatment. Inference strategy C1 was used (single sensor, independent blocks, background**
525 **concentration known). Statistics for runs with target heights 0.25 and 0.5 m and source width = 25 m are calculated.**
526 **All application periods are considered. Filled points show medians, boxes show interquartiles and bars show**
527 **minimums and maximums. Outliers are points to 1.5 times away from boxes limits.**

529

530 3.4.2 Effect of target heights on the bias

531 **Figure 10** shows that the bias remains **low** as long as sensor heights are low enough to catch a sufficient part of
532 the field footprint. When only a single height is used (strategy C1) this means that the sensor should be placed at
533 0.5 m or below for the field size we have tested here (25 m). **The result is similar for a pair of sensors**
534 **(strategy C3). For the lowest treatment though, the bias (and its variability) remain high whatever the**
535 **heights. It is interesting to notice that the heights which were found to provide an optimal inference of**
536 **NH₃ sources (below 0.5 m) are smaller than ZINST reported by Wilson et al. (1982) (which were 0.9 m for**
537 **40 m diameter circular sources, and which we estimate as 0.65 m based on a power law extrapolation as in**
538 **Laubach et al., 2012). It is also important to notice that this height should vary with both the roughness**
539 **length z_0 and displacement height as was showed by Wilson et al. (1982) for ZINST.**

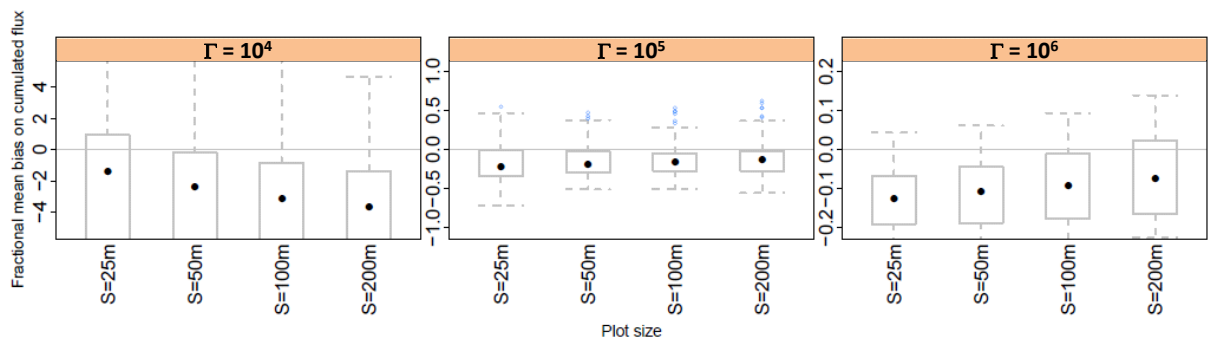


540
 541 **Figure 10.** Effect of target heights on source inference in a multiple-plot setup for integration periods of one week
 542 (168h). Same as the case reported for Figure 9 except that strategies C1 (with a single sensor, **top graphs**) and C3
 543 (with two heights, **bottom graphs**) are compared here (the background is assumed known in both strategies).

544

545 3.4.3. Effect of plot size on the bias

546 Increasing the plot size from 25 to 200 m width reduces the bias of the two **highest** source treatments for which
 547 the median bias reaches values around 10%, while the interquartiles remain stable (**Figure 11**). On the contrary,
 548 in treatment-1 ($\Gamma = 10^4$), the bias increases. It is expected that the bias in a multiple-source configuration never
 549 becomes smaller than the bias in a single source problem which is a limit linked to the time-integration
 550 (covariance between the source and the concentration, see **Eqns. 3 and 6**). It is also expected that the biases
 551 remain higher than the single source case until the source size increases sufficiently so that the concentration
 552 generated by a block on the neighbour fields become negligible compared to the concentration generated by the
 553 source below. This is what we observe in treatment-2 ($\Gamma = 10^5$) and treatment-3 ($\Gamma = 10^6$), with **treatment-2**
 554 showing a median bias of -13% (larger than in the single source case) for the 200 m **wide** field, while the bias of
 555 the **largest** source tends to be -10% [-17%, -1%], which is the range observed for a single source.



556
 557 **Figure 11.** Effect of plots size on source inference in a multiple-plot setup for integration periods of 168h and target
 558 heights 0.25 and 0.5 m. Same as in Figure 8.

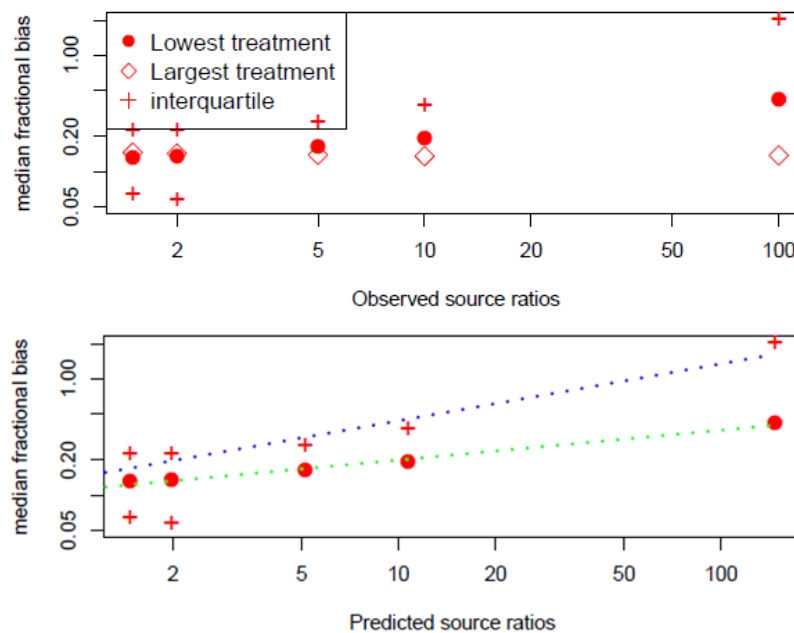
559

560 **3.4.4 Sensitivity of the method to ratios of emission potentials between treatments**

561 A central question is the capability of the inference method to resolve small or large differences in emissions
 562 from the nearby blocks. Indeed, we can speculate that small differences will be hard to resolve while large
 563 differences will lead to large bias. In order to determine the resolution power of the method, we compared the
 564 performance of the inference method with a set of three treatments: the first treatment had $\Gamma = 0$ to mimic a
 565 reference field receiving no nitrogen: the second treatment had a constant $\Gamma = 1000$ corresponding to a small
 566 emission ($0.7 \text{ kg N ha}^{-1} \text{ day}^{-1}$), while in the third treatment Γ was successively set to increasing values from 1500
 567 to 10^5 ($70 \text{ kg N ha}^{-1} \text{ day}^{-1}$). In this section we consider that the background is known (sensitivity to the
 568 background concentration will be evaluated in the next section).

569 **Figure 12** shows the median and interquartile biases of the cumulated emissions for the longest integration
 570 period 168h over the ratio of the high-to-low source treatments. The bias of the **largest** source always remained
 571 around 14%, which is larger than the single source case. The bias of the lowest source increased with increasing
 572 inter-treatments source ratio from 13% to 40%. In fact we find that the fractional bias increased approximately as
 573 a power function of the ratio of the two predicted sources (dotted lines, $0.11 x^{0.256}$).

574



575

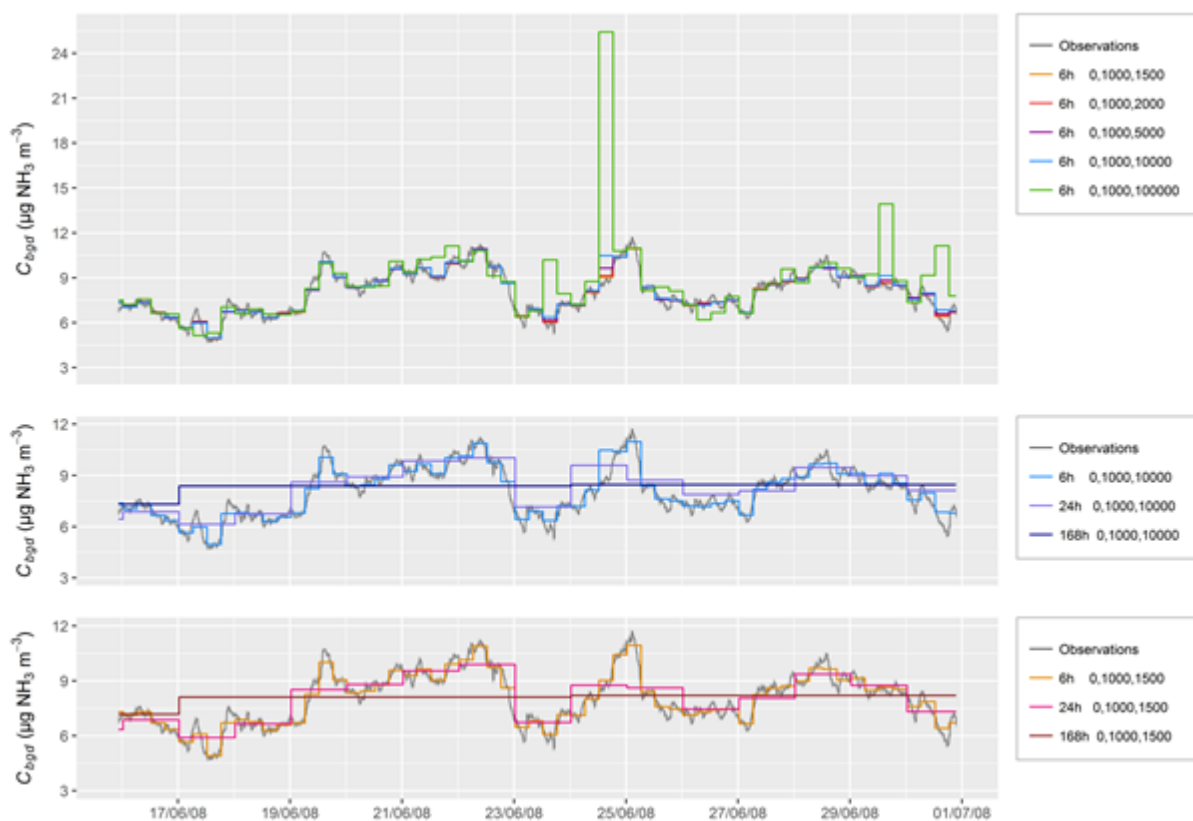
576 **Figure 12. Median fractional bias of cumulated emissions as a function of the ratio of the high-to-low source**
 577 **treatments for a 7 days integration period. Top: bias as a function of the theoretical source ratios. Bottom: bias as a**
 578 **function of the predicted source ratios. Dotted lines show power functions regressions on medians (green) and**
 579 **interquartile (blue). Strategies C1 and C3 are pooled together with all runs including sensor heights 0.25 and 0.5 m**

580

581 **3.4.5 Quality of background concentration estimations**

582 As pointed out by Flesch et al. (2004), the knowledge of the background concentration is essential in a source
 583 inference problem. Retrieving the background necessitates having at least $N_{\text{sources}}+1$ sensors. Hence only
 584 strategies with two heights per plot or which assume identical emissions in treatment repetitions can be evaluated
 585 in their capacity of retrieving the background (strategy C2 to C7). In order to evaluate the sensitivity of the
 586 method when the background concentration varies with time, we set a realistic background concentration as a

587 | linear combination of u_* and air temperature (T_a) with a mean of $6 \mu\text{g NH}_3 \text{ m}^{-3}$ and a standard deviation of
 588 | $0.1 \mu\text{g NH}_3 \text{ m}^{-3}$. This test was performed with a range of treatments in order to elucidate the correlations between
 589 | varying background and varying treatments. We see in **Figure 13** that the concentration, which follows a
 590 | realistic pattern, is well retrieved even over the longest **integration period of 168h**. However, we see that for the
 591 | treatments with the largest source contrast ($\Gamma = 1000$ and 10^5), the background concentration can be
 592 | overestimated even for small integration periods (6h). The median residual of the background concentration was
 593 | smaller in magnitude than $0.05 \mu\text{g NH}_3 \text{ m}^{-3}$, except for the case with very large differences between treatments
 594 | (0, 1000, 10000), for which the residual reached 0.1 and $0.5 \mu\text{g NH}_3 \text{ m}^{-3}$ for the 6h and 24h/168h integration
 595 | periods. Furthermore, the background concentrations were overestimated for the largest source ratios and
 596 | underestimated for the lowest source ratios and longer integration periods (24h and 168h).
 597



598
 599 | **Figure 13. Background concentrations prescribed (Observation) and inferred using strategy C7 and height**
 600 | **combination (0.25 m, 2 m): (a) effect of the treatment contrasts for a short integration period of 6h (treatments 1, 2**
 601 | **and 3 are given; (b) effect of integration period for contrasted treatments ($\Gamma = 0, 1000, 10000$); (c) effect of integration**
 602 | **period for similar treatments ($\Gamma = 0, 1000, 1500$).**

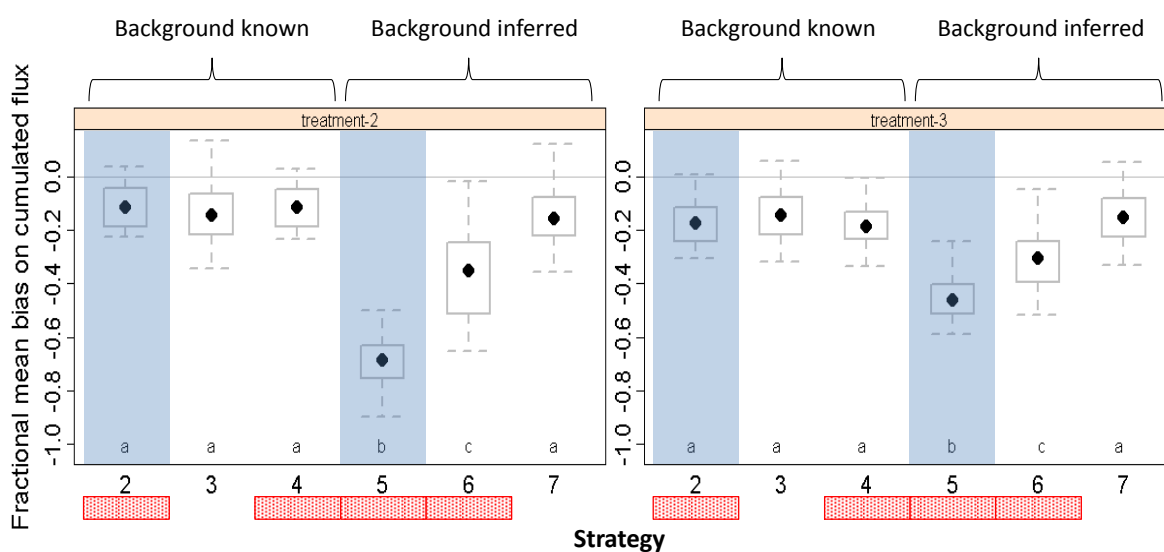
603

604 3.4.6 Identifying the most robust strategy

605 | Finally to identify which strategy is the most suitable for retrieving the emissions **from the multiplot**
 606 | **configuration, we compared** all strategies on a simulation with a variable background (set as in the previous
 607 | section) and two sources ratios of 2 and 20 between treatments 2 and 3 (treatment-1 **being** a zero source
 608 | reference). We found, as expected, that strategies with known backgrounds have low biases compared to
 609 | strategies that calculate the background, except for the strategy C7 which provided biases similar to strategy C3

610 which is the strategy equivalent to C7 but with known background (**Figure 14**). We also see that incorporating
 611 some knowledge of the sources by assuming plots from the same treatment have the same emissions, gave
 612 slightly better estimates when the background is known (strategies C2 and C4 compared to C3). This is however
 613 not true when the background is unknown, in which case the magnitude of the bias increases up to a median of
 614 0.7 (strategies C5 and C6 compared to C7). It is due to compensation between background concentration and
 615 source strength as we have seen in **Figure 14**, that the background concentration was overestimated in such
 616 cases. We also see, as expected, that the strategies with two sensors placed at different heights above each plot
 617 lead to better evaluations of the emissions. Overall, the strategy based on two sensors above each plot, which
 618 also assumes that sources are independent, seems to be the most robust (strategy C7). This strategy does not
 619 assume the background is known, nor does it assume the plots have similar emissions, which is more adapted to
 620 reality. Indeed, even though the same amount of nitrogen is applied in each repetition plot, the emission may
 621 vary due to soil heterogeneity and advection. We finally get a median bias for strategy C7 which is -16% with an
 622 interquartile [-8% -22%]. It is important to stress though that the minimums and maximums are further away,
 623 which indicates that under some rarer circumstances, the method may overestimate the sources by 12% or
 624 underestimate them by 40%. These cases correspond to integration periods with very low wind speeds and stable
 625 conditions.

626



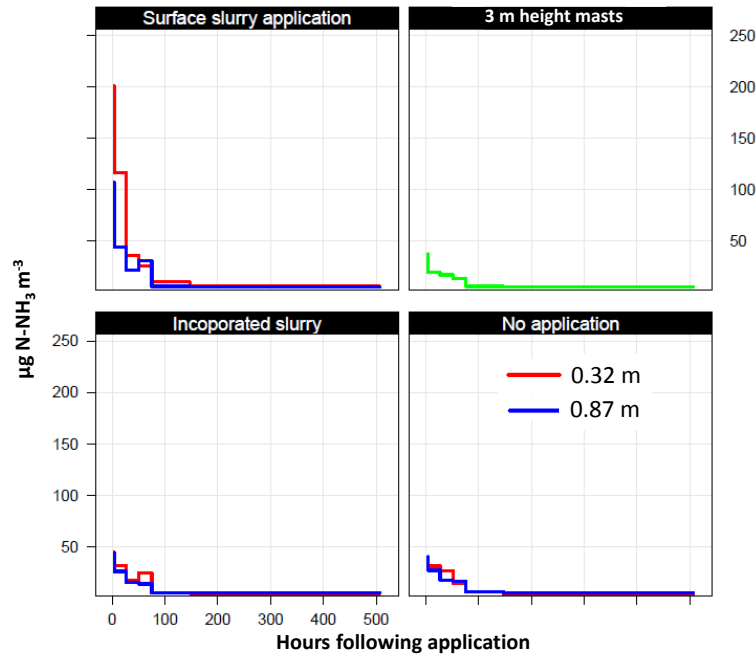
627

628 **Figure 14. Comparison of biases for all source inference strategies. In strategies C2, C3 and C4 we hypothesize that we**
 629 **have perfect knowledge of the background concentrations, while in strategies C5, C6 and C7 background**
 630 **concentrations are inferred together with the sources. In strategies C2, C4, C5 and C6 (red rectangles) we suppose**
 631 **that plots from the same treatment have the same emissions, while in strategy C3 and C7 we infer each plot**
 632 **separately. In strategy C2 and C5 we assume single sensors are placed above each plot (blue shades), while in**
 633 **strategies C3, C4, C6, C7 we assume two sensors are placed above each plot.**

634

635 3.5 Application of the methodology to a real test case with multiple treatments

636 The evaluation of the methodology on a real test case is shown in **Figures 15-17**. The concentration measured
 637 above the different treatments shows a much higher concentration above the surface applied slurry (up to
 638 200 $\mu\text{g N-NH}_3 \text{ m}^{-3}$) than above the two other treatments (below 50 $\mu\text{g N-NH}_3 \text{ m}^{-3}$), (**Figure 15**).

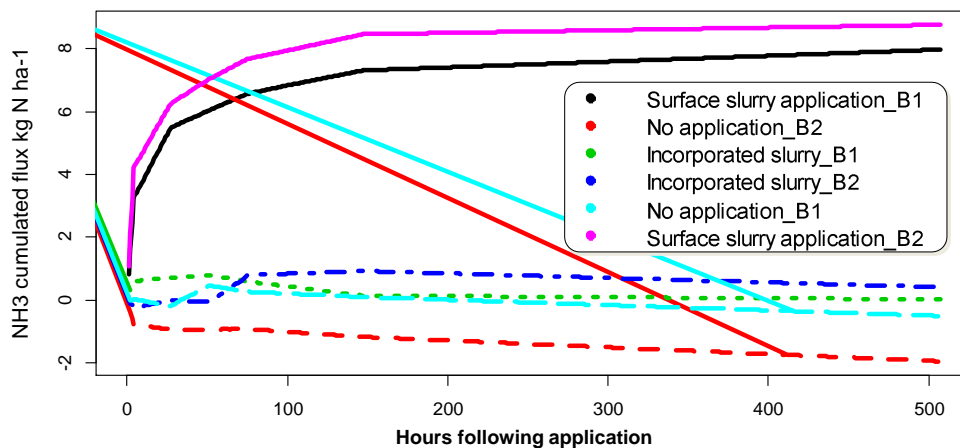


639

640 **Figure 15. Concentrations measured in a real test case with 6 blocks composed of three treatments and two**
 641 **repetitions. Here the mean concentration for the repetition and the three replicates ALPHA samplers are shown at**
 642 **two heights above ground. The concentration measured at 3 m height at 5 m away from the plots is also shown in**
 643 **green. The background concentration, evaluated as the minimum of the green curve was 5 µg N-NH₃ m⁻³.**

644

645 The inference method gives very consistent results both in terms of comparison between repetitions (**B1 and B2**)
 646 of a given treatment and in terms of comparison between treatments (Strategy C7 shown in **Figure 16**). Surface
 647 slurry application **showed the largest emissions: 9 ± 0.3 kg N ha⁻¹ in B1 and 10 ± 0.2 kg N ha⁻¹ in B2 (median**
 648 **and confidence interval)**. This corresponds to an emission factor around **24%** of the N-NH₄ applied and 8% of
 649 the total N applied, which is in-line with agronomic references (Sintermann et al., 2011a; Sommer et al., 2006).
 650 In contrast, the incorporated slurry showed much smaller **emissions: 0.3 ± 0.2 kg N ha⁻¹ in B1 and**
 651 **0.6 ± 0.2 kg N ha⁻¹ in B2. It is noticeable that the no-application showed slight deposition, especially in**
 652 **B2: -0.26 ± 0.2 kg N ha⁻¹ in B1 and -1.7 ± 0.2 kg N ha⁻¹ in B2.**

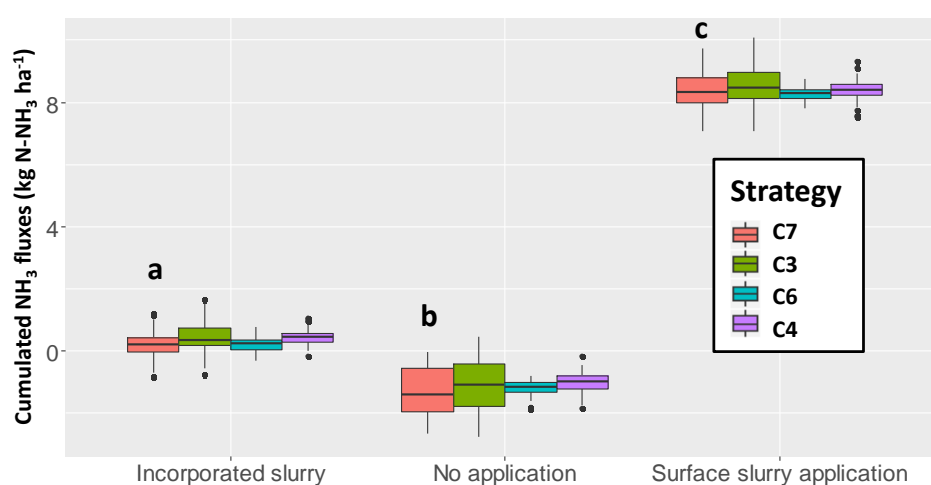


653

654 **Figure 16. Cumulated fluxes estimated with the inference method on the real test case with strategy C7. Three**
 655 **treatments with two repetitions are compared (b1 and B2).**

656

657 Comparing the inference strategies is instructive (**Figure 17**). We see that in methods which assume a known
 658 background (strategies C3 and C4), the inferred emissions are **slightly** higher than when background is assumed
 659 unknown. We should remind that we set the background concentration to the minimum concentration measured
 660 on the 3 m height masts because these were located too close to the plots to be considered as real background
 661 masts. This explains why strategies C3 and C4 lead to higher estimates compared to strategies C6 and C7, as the
 662 background may have been underestimated. We also find that all methods consistently infer a deposition flux to
 663 the blocks with no application, which is consistent with our knowledge of ammonia exchange between the
 664 atmosphere and the ground (Flechard et al., 2013). Indeed, the concentration in the atmosphere, which is
 665 enriched by the nearby sources is expected to be higher than near the ground, due to a low soil pH (6.1), a low
 666 nitrogen content in the soil surface ($6\text{-}9.5\text{ g N kg}^{-1}\text{ DM}$), and a 20% humid soil surface, hence leading to a flux
 667 from the air to the ground.



668
 669 **Figure 17.** Same as **Figure 16** but grouped by treatments and with additional strategies C4 and C6 which consider that
 670 replicates have the same surface flux. The variability in the boxplot aggregates the uncertainty on the inference
 671 method (the standard deviation on the flux estimate in the least-square model, which accounts for the variability in
 672 the replicated concentration measurements), and the variability between the repetitions in each treatment. **Letters a, b**
 673 **and c** shows significant differences between treatments for the C7 strategy, according to a Tukey test (95% family-
 674 wise confidence level).

675 From our theoretical study we know that strategy C7 should give a bias around $-16\% \pm \sim 7\%$. Therefore, we
 676 could expect that the real flux is the one measured with C7 times $1.15 (\pm 0.08)$, hence **would be 10.9 ± 1.3 kg N**
 677 **ha⁻¹**. This corresponds to $28 \pm 3\%$ of the N-NH₄ applied and $\sim 9 \pm 1\%$ of the total N applied. For the incorporated
 678 slurry, the **emissions are around 20 times smaller than the emissions from the surface applied slurry.**
 679 **Under these conditions, the bias on the emission would be around -20%, which means that the corrected**
 680 **emissions would range from 0.5% to 2.5% of the N-NH₄ applied and 0.2 and 0.8% of the total N applied.**
 681 We should bear in mind that the theoretical **correction** is based on the median of the simulations done with the
 682 2008 dataset in Grignon which had similar meteorological conditions to this trial. It would be much more
 683 relevant **though for** future developments to evaluate the bias based on the same method as developed here but
 684 **with** emissions and meteorological conditions **taken from** the real case.

685 3.6 Comparison with previous work

686 Several studies have reported methodologies for evaluating multiple sources using dispersion models. These
 687 were mostly based on backward Lagrangian modelling (Crenna et al., 2008; Flesch et al., 2009; Gao et al.,

688 2008). There were several inference methods reported: the methods based on the inversion of the dispersion
689 matrix D_{ij} or singular value decomposition of least-square optimisation (Flesch et al., 2009), which optimise the
690 conditioning of the dispersion matrix and one based on Bayesian inference (Yee and Flesch, 2010). Yee et al.
691 (2010) showed that the Bayesian approach would avoid unrealistic source estimates which could appear when
692 the matrix conditioning was poor. Unrealistic source estimates were for instance reported by Flesch et al. (2009),
693 with negative emission sources.

694 In Ro et al. (2011), they evaluated the bLS technique to infer two controlled methane surface sources with laser
695 measurements. They found 0.6 recovery ratios (ratio of inferred to known source) if the fields were not in the
696 footprint of the sensor but with adapted filters, they found a high degree of recovery with of 1.1 ± 0.2 and
697 0.8 ± 0.1 for the two sources respectively. They found that in contradiction to Crenna et al. (2008) and Flesch et
698 al. (2009), even with large conditioning numbers they had high recovery rates.

699 **Misselbrook (2005) compared different methodologies and showed that under high concentrations**
700 **diffusion samplers may lead to overestimation of up to 70% of the concentration. They suggest potential**
701 **issues related to the deformation of the Teflon membrane which would modify the distance between**
702 **coated filters and the membrane itself that could cause sampler saturation. There is hence some concern**
703 **on the quality of diffusion samplers to measure concentrations at heights close to large sources which**
704 **would necessitate field validations.**

705 3.6.1 Sensor positioning and conditioning number

706 Crenna et al. (2008) have clearly shown that the optimal sensor positioning should be so that each sensor sees
707 preferentially a single source, and reversely, each source should preferentially influence a single sensor. In this
708 study the sources-sensors geometry was especially designed in a way that minimises the condition number CN ,
709 by placing the sensors in the middle of each plot. For the smallest source ($x_{plot} = 25$ m), the conditioning number
710 ranged from 1.97 to 3.01 (median 2.42) for sensors located at 0.25 m, and increased to 2.6-6.9 (median 3.2) for
711 sensors at 0.5 m, 4.7-150 (median 21) for sensors at 1.0 m, and 40-165000 (median 640) for sensors at 2 m. This
712 shows that including at least one sensor per block at heights lower than the field width divided by 20 would
713 ensure that the conditioning number remains lower than in most trials **reported by** Crenna et al. (2008).

714 By comparing different strategies we have found that the strategies using two sensors over each source
715 systematically led to improved performances (C3 versus C1 and C6 versus C5, **Figure 14**). This is also in line
716 with the results of Crenna et al. (2008), who showed that using more sensors separated spatially improves the
717 performance of the inference method. Hence we can conclude that the inference method we used is based on a
718 well-conditioned system which leads to robust results of the least-square optimisation. This is further illustrated
719 by the real case example (**Figures 15-17**) which shows a good reproducibility between block repetitions. Indeed,
720 good reproducibility between repetitions is a check for evaluating the quality of the inference method in real test
721 cases. The use of Bayesian inference method would however also be valuable in the setup we propose here.

722 3.6.2 Effect of time integrating sensors on the source inference quality

723 The use of time averaging sensors for estimating ammonia sources was already reported by Sanz et al. (2010),
724 Theobald et al. (2013), Carozzi et al. (2013a; 2013b), Ferrara et al. (2014) and Riddick et al. (2016a; 2014). All
725 these studies have shown the feasibility of these measurements, however only a few of them allow estimating the

726 impact of averaging: Riddick et al. (2014) measured emissions from a bird colony in the Ascension Island with
727 WindTrax using both several ALPHA samplers in a transect across the colony and a continuous analyser for
728 ammonia (AiRRmonia, Mechatronics, NL) downwind. They also averaged the continuous sampler
729 concentrations to evaluate the effect of averaging on the emissions estimates. They found as we do here that
730 averaging over monthly periods would lead to systematic underestimations from -9% to -66%. They also found
731 that estimations from **diffusive samplers** would lead to average underestimations of -12%. This is very close to
732 what we find here for a single source over one week (**Figure 6**). In a similar comparison Riddick et al. (2016b)
733 found that time-integration led to slight overestimations with integration approach, which is within the range of
734 statistics of the bias we have found for the larger area sources (3rd quartile in **Figure 6**).

735 **3.6.3 Dependency to meteorological conditions**

736 We should bear in mind that the use of time averaging sensors in the inference method is also highly dependent
737 on the surface layer turbulent structure as shown by **Figure 7**. We find, as expected, that stable conditions or low
738 wind speed conditions are those that lead to the highest potential bias (as shown by the 3rd quartile under stable
739 conditions in **Figure 7** bottom). This is a well-known limitation of inverse dispersion modelling which was
740 reported by Flesch et al. (2009; 2004) and which suggested that inverse dispersion would be inaccurate for
741 $u_* < 0.15 \text{ m s}^{-1}$ and $|z/L| < 1$. However, both our study and the studies of Riddick et al. (2014; 2016b) show that
742 this is not as much of an issue for ammonia emissions. Indeed, this is due to the fact that ammonia emissions
743 follow a daily cycle with low emissions at night and high emissions during the day. This is firstly because the
744 ground surface compensation point concentration ($C_{p\text{ground}}$) has an exponential dependency on surface
745 temperature as assumed in **Eq. (10)** based on known thermodynamical equilibrium constants (Flechard et al.,
746 2013). This is secondly due to the fact that ammonia emission is a diffusion-based process which is limited by
747 the surface resistances, as modelled in **Eq. (9)**, which leads to small fluxes when $R_a(z_{ref})$ and $R_{b\text{NH}_3}$ get large,
748 which happens during low wind speeds (they are both roughly inversely proportional to wind speed) and stable
749 conditions, which also happens at night (Flechard et al., 2013). In real situations, the combination of small
750 turbulence and high surface concentration leads to a further decrease of the flux which is dependent on the
751 difference between $C_{p\text{ground}}$ and the concentration in the atmosphere above (a feature which was not accounted
752 for in this study as this would imply a higher degree of complexity in the modelling approach). This means that
753 the results we found in this study would not apply for species having an emission pattern with a different
754 temporal dynamics (either constant or anti-correlated with surface temperature or wind speed).

755 **4. Conclusions**

756 In this study we have demonstrated that it is possible to infer with reasonable biases ammonia emissions from
757 multiple small fields located near each other using a combination of a dispersion model and a set of passive
758 diffusion sensors which integrate over a few hours to weekly periods. We found that the Philip (1959) analytical
759 model **in FIDES** gave similar concentrations as the backward Lagrangian Stochastic model WindTrax **at 2 m**
760 **above a small source, under neutral and stable stratification** as long as the stability correction functions used
761 in both models are similar **and the Schmidt number is identical (here set to 0.64). Under unstable conditions**
762 **FIDES gave 20% smaller concentrations at 2 m compared to WindTrax.**

763 We demonstrated by theoretical considerations that passive sensors always lead to the underestimation of
764 ammonia emissions for an isolated source because of the negative time correlation between the ammonia
765 emissions and the transfer function. Using a yearly meteorological dataset typical of the oceanic climate of
766 western Europe we found that the bias over weekly integration times is typically $-8\pm 6\%$, which is in line with
767 previous reports. Larger biases are expected for meteorological conditions with stable conditions and low wind
768 speeds as soon as the integration period is larger than 12 hours.

769 We showed that the quality of the inference method for multiple sources was dependent on the number of
770 sensors considered above each plot. The most essential technique to minimise the bias of the method was to
771 place a sensor in the middle of each source within the boundary layer. The quality of the sensor positioning was
772 evaluated using “condition numbers” which ranged from 2 to 3 for a sensor placed at 25 cm above the ground to
773 much higher values ($40-1.6\times 10^5$) for a sensor at 2 m height above 25 m width sources. **Although the lowest
774 sensors have the best condition number, we would rather recommend using heights of 50 cm above the
775 canopy in order to reduce uncertainty in positioning the sensors close to the ground as well as avoid non-
776 diffusive transfer conditions. Similarly,** although the highest sensors had low condition numbers, they were
777 shown to improve the robustness of the sources inference especially for evaluating the background
778 concentrations. Using replicates of each treatment was found to be essential for evaluating the quality of the
779 inference and derive robust statistical indicators for each treatment.

780 When considering a system, characteristic of agronomic trials, composed of a low and a high potential source
781 and a reference with no nitrogen application, we found that the fractional bias remained smaller than around 25%
782 for ratios between the largest to the smallest sources lower than factor 5 and increased as a power function of the
783 ratio. Furthermore, the dynamics of the emissions were found not to strongly affect the fractional bias. As
784 expected, we also found that the fractional bias decreased with increasing source dimensions, especially for the
785 lowest source strength in a multiple source trial.

786 Finally, a test on a practical trial proved the applicability of the method in real situations with contrasted
787 emissions. We indeed calculated ammonia emissions of around $27 \pm 3\%$ of the total ammoniacal nitrogen
788 applied for surface applied slurry while we found less than 1% emissions for the treatments with incorporated
789 slurry.

790 This method could also be improved by incorporating knowledge of the surface source dynamics into the
791 inference procedure. Further work is required however, for validating the method, for instance using prescribed
792 emissions, and to evaluate it for growing crops using real measurements with diffusion samplers close to the
793 ground.

794 **Acknowledgements**

795 This study was supported by EU FP7 NitroEurope-IP (grant number 017841) and ECLAIRE (grant number
796 282910), French national projects CASDAR VOLAT’NH₃ (grant number 0933), ADEME EVAPRO (grant
797 number 1560C0036), ADEME EVAMIN (grant number 1660C0012). The data sets used in this paper can be
798 obtained from the authors upon request. The meteorological dataset used in this study are from the ICOS site FR-
799 GRI which can be obtained from <http://fluxnet.fluxdata.org/>. We thank Erwan Personne for the use of the
800 SurfAtm-NH₃ model, **and the technical team of the ARVALIS research station of “La Jaillière” for their
801 involvement in the conduct of the “real test case” experiment.**

802 **Supplementary material**

803 See supplementary material manuscript

804 **Model availability**

805 **The model is available as an R package upon request to the authors.**

806 **References**

- 807 Carozzi, M., Ferrara, R.M., Rana, G. and Acutis, M., 2013a. Evaluation of mitigation strategies to reduce
808 ammonia losses from slurry fertilisation on arable lands. *Sci Total Environ*, 449: 126-33.
- 809 Carozzi, M., Loubet, B., Acutis, M., Rana, G. and Ferrara, R.M., 2013b. Inverse dispersion modelling highlights
810 the efficiency of slurry injection to reduce ammonia losses by agriculture in the Po Valley (Italy).
811 *Agric. For. Meteorol.*, 171: 306-318.
- 812 Choudhury, B.J. and Monteith, J.L., 1988. A four-layer model for the heat budget of homogeneous land surfaces.
813 *Q.J.R. Meteorol. Soc.*, 114: 373-398.
- 814 CITEPA, 2017. Inventaire des émissions de polluants atmosphériques en France métropolitaine, format CEE-
815 NU. CITEPA 494 / Convention MATE 26 / 2001, Centre Interprofessionnel Technique d'Etudes de la
816 Pollution Atmosphérique.
- 817 Council, E., 1996. Directive 96/61/EC of 24th September 1996 concerning integrated pollution prevention and
818 control. , European Council, Brussels, Belgium.
- 819 Council, E., 2016. Directive (EU) 2016/2284 of the European parliament and of the council of 14 December
820 2016 on the reduction of national emissions of certain atmospheric pollutants, amending Directive
821 2003/35/EC and repealing Directive 2001/81/EC, European Council, Brussels, Belgium.
- 822 Crenna, B.R., Flesch, T.K. and Wilson, J.D., 2008. Influence of source-sensor geometry on multi-source
823 emission rate estimates. *Atmos. Environ.*, 42(32): 7373-7383.
- 824 ECETOC, 1994. Ammonia emissions to air in Western Europe, European Centre for Ecotoxicology and
825 Toxicology of Chemicals, Avenue E Van Nieuwenhuysse 4, Brussels.
- 826 EUROSTAT, 2012. Agroenvironmental indicator - ammonia emission, Eurostat, Luxemburg.
- 827 Faburé, J. et al., 2011. Synthèse bibliographique sur la contribution de l'agriculture à l'émission de particules
828 vers l'atmosphère : identification de facteurs d'émission, ADEME / INRA.
- 829 Famulari, D. et al., 2010. Development of a low-cost system for measuring conditional time-averaged gradients
830 of SO₂ and NH₃. *Environ Monit Assess*, 161(1-4): 11-27.
- 831 Ferrara, R.M. et al., 2016. Dynamics of ammonia volatilisation measured by eddy covariance during slurry
832 spreading in north Italy. *Agriculture, Ecosystems & Environment*, 219: 1-13.
- 833 Ferrara, R.M. et al., 2014. Ammonia volatilisation following urea fertilisation in an sorghum crop in Italy
834 irrigated. *Agric. For. Meteorol.*, 195: 179-191.
- 835 Ferrara, R.M. et al., 2012. Eddy covariance measurement of ammonia fluxes: Comparison of high frequency
836 correction methodologies. *Agric. For. Meteorol.*, 158(0): 30-42.
- 837 Flechard, C.R. and Fowler, D., 1998. Atmospheric ammonia at a moorland site. II: Long-term surface-
838 atmosphere micrometeorological flux measurements. *Q.J.R. Meteorol. Soc.*, 124(547): 759-791.
- 839 Flechard, C.R. et al., 2013. Advances in understanding, models and parameterizations of biosphere-atmosphere
840 ammonia exchange. *Biogeosciences*, 10(7): 5183-5225.
- 841 Flesch, T.K., Harper, L.A., Desjardins, R.L., Gao, Z.L. and Crenna, B.P., 2009. Multi-Source Emission
842 Determination Using an Inverse-Dispersion Technique. *Boundary-Layer Meteorology*, 132(1): 11-30.
- 843 Flesch, T.K., Wilson, J.D., Harper, L.A., Crenna, B.P. and Sharpe, R.R., 2004. Deducing ground-to-air
844 emissions from observed trace gas concentrations: A field trial. *J. Appl. Meteorol.*, 43(3): 487-502.
- 845 Flesch, T.K., Wilson, J.D. and Yee, E., 1995. Backward-Time Lagrangian Stochastic Dispersion Models and
846 Their Application to Estimate Gaseous Emissions. *J. Appl. Meteorol.*, 34(6): 1320-1332.
- 847 Gao, Z.L., Desjardins, R.L., van Haarlem, R.P. and Flesch, T.K., 2008. Estimating Gas Emissions from Multiple
848 Sources Using a Backward Lagrangian Stochastic Model. *Journal of the Air & Waste Management
849 Association*, 58(11): 1415-1421.
- 850 Gao, Z.L., Mauder, M., Desjardins, R.L., Flesch, T.K. and van Haarlem, R.P., 2009. Assessment of the backward
851 Lagrangian Stochastic dispersion technique for continuous measurements of CH₄ emissions. *Agric.
852 For. Meteorol.*, 149(9): 1516-1523.

853 Gericke, D., Pacholski, A. and Kage, H., 2011. Measurement of ammonia emissions in multi-plot field
854 experiments. *Biosystems Engineering*, 108(2): 164-173.

855 Häni, C., Sintermann, J., Kupper, T., Jocher, M. and Neftel, A., 2016. Ammonia emission after slurry application
856 to grassland in Switzerland. *Atmospheric Environment*, 125(Part A): 92-99.

857 Holtslag, A.A.M. and Vanulden, A.P., 1983. A Simple Scheme for Daytime Estimates of the Surface Fluxes
858 from Routine Weather Data. *Journal of Climate and Applied Meteorology*, 22(4): 517-529.

859 Huang, C.H., 1979. A theory of dispersion in turbulent shear flow. *Atmos. Environ.*, 13: 453-463.

860 Kaimal, J.C. and Finnigan, J.J., 1994. *Atmospheric Boundary Layer Flows, Their structure and measurement.*
861 Oxford University Press., New York, 289 pp.

862 Kormann, R. and Meixner, F.X., 2001. An analytical footprint model for non-neutral stratification. *Boundary*
863 *Layer Meteorol.*, 99(2): 207-224.

864 Laubach, J., Taghizadeh-Toosi, A., Sherlock, R.R. and Kelliher, F.M., 2012. Measuring and modelling ammonia
865 emissions from a regular pattern of cattle urine patches. *Agric. For. Meteorol.*, 156: 1-17.

866 Loubet, B. et al., 2012. Investigating the stomatal, cuticular and soil ammonia fluxes over a growing tritical crop
867 under high acidic loads. *Biogeosciences*, 9(4): 1537-1552.

868 Loubet, B. et al., 2010. An inverse model to estimate ammonia emissions from fields. *European Journal of Soil*
869 *Science*, 61(5): 793-805.

870 Loubet, B., Milford, C., Sutton, M.A. and Cellier, P., 2001. Investigation of the interaction between sources and
871 sinks of atmospheric ammonia in an upland landscape using a simplified dispersion-exchange model. *J.*
872 *Geophys. Res.-Atmos.*, 106(D20): 24183-24195.

873 Lushi, E. and Stockie, J.M., 2010. An inverse Gaussian plume approach for estimating atmospheric pollutant
874 emissions from multiple point sources. *Atmos. Environ.*, 44(8): 1097-1107.

875 McGinn, S.M. and Janzen, H.H., 1998. Ammonia sources in agriculture and their measurement. *Canadian*
876 *Journal of Soil Science*, 78(1): 139-148.

877 Milford, C., Hargreaves, K.J., Sutton, M.A., Loubet, B. and Cellier, P., 2001. Fluxes of NH₃ and CO₂ over
878 upland moorland in the vicinity of agricultural land. *J. Geophys. Res.-Atmos.*, 106(D20): 24169-24181.

879 Milford, C. et al., 2009. Ammonia fluxes in relation to cutting and fertilization of an intensively managed
880 grassland derived from an inter-comparison of gradient measurements. *Biogeosciences*, 6(5): 819-834.

881 Misselbrook, T.H., Nicholson, F.A., Chambers, B.J. and Johnson, R.A., 2005. Measuring ammonia emissions
882 from land applied manure: an intercomparison of commonly used samplers and techniques.
883 *Environmental Pollution*, 135(3): 389-397.

884 Moring, A. et al., 2016. A process-based model for ammonia emission from urine patches, GAG (Generation of
885 Ammonia from Grazing): description and sensitivity analysis. *Biogeosciences*, 13(6): 1837-1861.

886 Mukherjee, S., McMillan, A.M.S., Sturman, A.P., Harvey, M.J. and Laubach, J., 2015. Footprint methods to
887 separate N₂O emission rates from adjacent paddock areas. *International Journal of Biometeorology*,
888 59(3): 325-338.

889 Nemitz, E. et al., 2009. Aerosol fluxes and particle growth above managed grassland. *Biogeosciences*, 6(8):
890 1627-1645.

891 Nemitz, E., Sutton, M.A., Schjoerring, J.K., Husted, S. and Wyers, G.P., 2000. Resistance modelling of
892 ammonia exchange over oilseed rape. *Agricultural and Forest Meteorology*, 105(4): 405-425.

893 Pacholski, A. et al., 2006. Calibration of a simple method for determining ammonia volatilization in the field -
894 comparative measurements in Henan Province, China. *Nutrient Cycling in Agroecosystems*, 74(3): 259-
895 273.

896 Personne, E. et al., 2009. SURFATM-NH₃: a model combining the surface energy balance and bi-directional
897 exchanges of ammonia applied at the field scale. *Biogeosciences*, 6(8): 1371-1388.

898 Personne, E. et al., 2015. Investigating sources and sinks for ammonia exchanges between the atmosphere and a
899 wheat canopy following slurry application with trailing hose. *Agricultural and Forest Meteorology*, 207:
900 11-23.

901 Philip, J.R., 1959. The Theory of Local Advection .1. *J Meteorol*, 16(5): 535-547.

902 Riddick, S. et al., 2016a. Estimate of changes in agricultural terrestrial nitrogen pathways and ammonia
903 emissions from 1850 to present in the Community Earth System Model. *Biogeosciences*, 13(11): 3397-
904 3426.

905 Riddick, S.N. et al., 2014. Measurement of ammonia emissions from tropical seabird colonies. *Atmos. Environ.*,
906 89: 35-42.

907 Riddick, S.N. et al., 2016b. Measurement of ammonia emissions from temperate and sub-polar seabird colonies.
908 *Atmos. Environ.*, 134: 40-50.

909 Ro, K.S., Johnson, M.H., Hunt, P.G. and Flesch, T.K., 2011. Measuring Trace Gas Emission from Multi-
910 Distributed Sources Using Vertical Radial Plume Mapping (VRPM) and Backward Lagrangian
911 Stochastic (bLS) Techniques. *Atmosphere*, 2(3): 553-566.

912 Sanz, A., Misselbrook, T., Sanz, M.J. and Vallejo, A., 2010. Use of an inverse dispersion technique for
913 estimating ammonia emission from surface-applied slurry. *Atmos. Environ.*, 44(7): 999-1002.

914 Sintermann, J. et al., 2011a. Determination of field scale ammonia emissions for common slurry spreading
915 practice with two independent methods. *Atmos. Meas. Tech.*, 4(9): 1821-1840.

916 Sintermann, J. et al., 2012. Are ammonia emissions from field-applied slurry substantially over-estimated in
917 European emission inventories? *Biogeosciences*, 9(5): 1611-1632.

918 Sintermann, J. et al., 2011b. Eddy covariance flux measurements of ammonia by high temperature chemical
919 ionisation mass spectrometry. *Atmos. Meas. Tech.*, 4(3): 599-616.

920 Sommer, S.G. et al., 2003. Processes controlling ammonia emission from livestock slurry in the field. *European*
921 *Journal of Agronomy*, 19(4): 465-486.

922 Sommer, S.G., Jensen, L.S., Clausen, S.B. and SØgaard, H.T., 2006. Ammonia volatilization from surface-
923 applied livestock slurry as affected by slurry composition and slurry infiltration depth. *The Journal of*
924 *Agricultural Science*, 144(3): 229-235.

925 Sommer, S.G., McGinn, S.M. and Flesch, T.K., 2005. Simple use of the backwards Lagrangian stochastic
926 dispersion technique for measuring ammonia emission from small field-plots. *European Journal of*
927 *Agronomy*, 23(1): 1-7.

928 Spirig, C., Flechard, C.R., Ammann, C. and Neftel, A., 2010. The annual ammonia budget of fertilised cut
929 grassland - Part 1: Micrometeorological flux measurements and emissions after slurry application.
930 *Biogeosciences*, 7(2): 521-536.

931 Sun, K. et al., 2015. Open-path eddy covariance measurements of ammonia fluxes from a beef cattle feedlot.
932 *Agricultural and Forest Meteorology*, 213: 193-202.

933 Sutton, M.A. et al., 2001. Comparison of low cost measurement techniques for long-term monitoring of
934 atmospheric ammonia. *J Environ Monit*, 3(5): 446-53.

935 Sutton, M.A. et al., 2009. Dynamics of ammonia exchange with cut grassland: synthesis of results and
936 conclusions of the GRAMINAE Integrated Experiment. *Biogeosciences*, 6(12): 2907-2934.

937 Sutton, M.A. et al., 2011. Too much of a good thing. *Nature*, 472(7342): 159-161.

938 Sutton, M.A. et al., 2013. Towards a climate-dependent paradigm of ammonia emission and deposition. *Philos*
939 *Trans R Soc Lond B Biol Sci*, 368(1621): 20130166.

940 Tang, Y.S., Cape, J.N. and Sutton, M.A., 2001. Development and types of passive samplers for monitoring
941 atmospheric NO₂ and NH₃ concentrations. *TheScientificWorldJournal*, 1: 513-29.

942 Tang, Y.S. et al., 2009. European scale application of atmospheric reactive nitrogen measurements in a low-cost
943 approach to infer dry deposition fluxes. *Agriculture Ecosystems & Environment*, 133(3-4): 183-195.

944 Theobald, M.R., Crittenden, P.D., Tang, Y.S. and Sutton, M.A., 2013. The application of inverse-dispersion and
945 gradient methods to estimate ammonia emissions from a penguin colony. *Atmos. Environ.*, 81: 320-
946 329.

947 Thomson, L.C. et al., 2007. An improved algorithm for locating a gas source using inverse methods. *Atmos.*
948 *Environ.*, 41(6): 1128-1134.

949 UNECE (Editor), 2012. 1999 Protocol to Abate Acidification, Eutrophication and Ground-level Ozone to the
950 Convention on Long-range Transboundary Air Pollution, as amended on 4 May 2012
951 (http://www.unece.org/env/lrtap/multi_h1.html). UNECE, Brussels, Belgium.

952 Van der Hoven, I., 1957. Power Spectrum of Horizontal Wind Speed in the Frequency Range from 0.0007 to 900
953 Cycles Per Hour. *Journal of Meteorology*, 14(2): 160-164.

954 Vandré, R. and Kaupenjohann, M., 1998. In Situ Measurement of Ammonia Emissions from Organic Fertilizers
955 in Plot Experiments. *Soil Science Society of America Journal*, 62(2): 467-473.

956 Wang, W., Liu, W.Q., Zhang, T.S. and Ren, M.Y., 2013. Evaluation of backward Lagrangian stochastic (bLS)
957 model to estimate gas emissions from complex sources based on numerical simulations. *Atmos.*
958 *Environ.*, 67: 211-218.

959 Whitehead, J.D. et al., 2008. Evaluation of laser absorption spectroscopic techniques for eddy covariance flux
960 measurements of ammonia. *Environ Sci Technol*, 42(6): 2041-6.

961 Wilson, J.D., 2015. Computing the Flux Footprint. *Boundary Layer Meteorol.*, 156(1): 1-14.

962 Wilson, J.D. and Shum, W.K.N., 1992. A Reexamination of the Integrated Horizontal Flux Method for
963 Estimating Volatilization from Circular Plots. *Agric. For. Meteorol.*, 57(4): 281-295.

964 Wilson, J.D., Thurtell, G.W., Kidd, G.E. and Beauchamp, E.G., 1982. Estimation of the rate of gaseous mass
965 transfer from a surface source plot to the atmosphere. *Atmospheric Environment (1967)*, 16(8): 1861-
966 1867.

967 Yee, E., 2008. Theory for reconstruction of an unknown number of contaminant sources using probabilistic
968 inference. *Boundary Layer Meteorol.*, 127(3): 359-394.

969 Yee, E. and Flesch, T.K., 2010. Inference of emission rates from multiple sources using Bayesian probability
970 theory. *J Environ Monit*, 12(3): 622-34.

971

1 Supplementary material: Evaluation of a new inference 2 method for estimating ammonia volatilisation from multiple 3 agronomic plots

4 Benjamin Loubet^{1,*}, Marco Carozzi^{1,#}, Polina Voylokov¹, Jean-Pierre Cohan², Robert
5 Trochard², Sophie Générmont¹

6 1 INRA, UMR ECOSYS, INRA, AgroParisTech, Université Paris-Saclay, 78850, Thiverval-Grignon, France

7 2 ARVALIS-Institut du Végétal, **Station expérimentale de La Jaillière, La Chapelle Saint Sauveur, 44370**
8 **Loireauxence**, France

9 # now at: Agroscope Research Station, Climate and **Agriculture**, Zurich, Switzerland

10 * Corresponding author: Benjamin.Loubet@inra.fr

11 S1. Analogy between dispersion equation and flux-resistance approaches

12 It is interesting to note that **Eq. (1)** is essentially similar to resistance analogy approaches, where the flux F is
13 evaluated as a concentration difference divided by a transfer resistance between two heights z_1 and z_2 , $F =$
14 $-(C(z_2) - C(z_1))/R(z_1, z_2)$. Indeed, assuming, as is done in the resistance analogy that the source is infinitely
15 expanded in x , then computing **Eq. (1)** for heights z_1 and z_2 and recombining leads simply to $R(z_1, z_2) =$
16 $D(z_1) - D(z_2)$. Hence the transfer function D is equivalent to a transfer resistance. In particular, for infinitely
17 expanded sources, the resistance between two heights equals the difference between the transfer function
18 between these two heights and the ground.

19 S2 Condition number to identify suitable source-receptor geometry

20 A major issue when trying to infer sources from **atmospheric** concentrations is the fact that under some
21 circumstances, the problem is ill-conditioned, which means that a small change in the concentration or the
22 transfer matrix D_{ij} will induce large changes on the sources strength estimates. A measure of the conditioning of
23 the problem is therefore an important indicator for determining whether the source-receptor geometry can lead to
24 realistic solutions. The condition number is a measure of ill-conditioning and is defined as (Crenna et al., 2008):

$$26 \quad CN = \|D_{ij}\| \times \|D_{ij}^{-1}\| \quad (S1)$$

27
28 Where $\|\cdot\|$ denotes a norm of **the** matrix, one definition of which being the maximum of the sum of the rows.
29 The higher CN , the larger the uncertainty on the solution of **Eqns. (3)** and **(6)** (Flesch et al., 2009). To evaluate
30 the conditioning state of each set-up, we considered the simplified case where the background concentration is
31 zero and the number of receptors equals the number of sources. In such a case, the matrix D_{ij} is squared and D_{ij}^{-1}
32 is defined.

33 Considering the single source case eases the understanding of the **meaning of** condition number. Indeed, in that
34 case $D_{ij} = D_j$ is a vector and CN is simply: $\max(\overline{D(x_i)})/\min(\overline{D(x_i)})$. In physical terms, this means that if
35 some concentration samplers are well exposed to the source and others are not, CN is large. In such a case, **Eq.**

Code de champ modifié

36 (4) shows that the a small error in $\overline{C(x_i)} - \overline{C_{bgd}}$ will lead to a large error in \overline{S} . Therefore we see here that using
37 several concentration samplers may lead to increasing the error on \overline{S} if their locations are not chosen with care.
38 This was also showed by Crenna et al. (2008) and Flesch et al. (2009), who showed that the condition
39 number CN should be minimised in order to keep this error minimal; in this regards, Gao et al. (2008) suggest
40 that CN should be smaller than 10. In practice, minimising CN would mean minimising the range of $\overline{D(x_i)}$. **We**
41 **can interpret this in terms of footprint**: the source area should represent a reasonable footprint fraction of each
42 concentration sensor. This holds for multiple sources also: in that case each source should represent a large
43 fraction of each sensor footprint placed above it. The setup we propose in this study is, by construction,
44 minimising CN as the sensors are placed in the middle of each plot, provided they are placed low enough to
45 catch a significant part of the field footprint. If the plots are in a non-squared configuration, the CN is simply
46 calculated as in **Eq. S1**, where the second term in the right hand **side** is the pseudo inverse of the matrix D_{ij} . **In**
47 **practice**, the calculation of CN was performed **using** the kappa function in R (version 3.2.3).

48 S3. Details of the FIDES model based on a solution of Philip (1959) of the advection diffusion equation

49 In the FIDES model, the transfer function $D(x_i, S_j, t)$ was estimated by first translating and rotating the x-y plan
50 to locate the source S_j at the centre coordinates (0,0) and set the wind direction WD to 0 (align the x-axis with the
51 wind vector. This was done by setting the following coordinate transformation $X_{ij} = (x_i - x_{s_j}) \sin(WD) -$
52 $(y_i - y_{s_j}) \cos(WD)$, and $Y_{ij} = (x_i - x_{s_j}) \cos(WD) - (y_i - y_{s_j}) \sin(WD)$. Moreover, all heights are
53 considered as heights above displacement height d ($Z = z - d$). In such conditions, the Philip (1959) solution
54 reads:

$$55 U(Z_i) = aZ_i^p \quad (S2)$$

$$56 K_z(Z_i) = bZ_i^n \quad (S3)$$

$$57 D(x_i, S_j, t) = \frac{1}{\sigma_y(X_{ij})\sqrt{2\pi}} \exp\left(-\frac{(Y_{ij})^2}{2\sigma_y^2}\right) \times \frac{(Z_i Z_s)^{(1-n)/2}}{b\alpha X_{ij}} \times \exp\left(-\frac{a(Z_i^\alpha + Z_s^\alpha)}{b\alpha^2 X_{ij}}\right) \times I_{-v}\left(\frac{2a(Z_i Z_s)^{\alpha/2}}{b\alpha^2 X_{ij}}\right) \quad (S4)$$

$$58 \sigma_y = \frac{1}{\sqrt{2}} C_y X_{ij}^{\frac{2-m}{2}}$$

59 where $\alpha = 2 + p + n$, $v = (1 - n) / \alpha$, and I_{-v} is the modified Bessel function of the first kind of order $-v$, and C_y
60 and m were taken from Sutton (1932). The values of a , b , p and n were inferred by linear regression between
61 $\ln(U)$, $\ln(K_z)$ and $\ln(Z)$, over the height range $2 \times z_0$ to 20 m, using $U(z)$ and $K_z(z)$ estimated from the Monin-
62 Obukhov similarity theory as $K_z(Z) = k u_* Z [Sc\phi_H(Z/L)]^{-1}$. Here $\phi_H(Z/L)$ is the universal stability correction
63 function as in Kaimal and Finnigan (1994), which is $\phi_H(Z/L) = (1 + 5.2 Z/L)$ for $Z/L \geq 0$ and $\phi_H(Z/L) =$
64 $(1 - 16 Z/L)^{0.5}$ for $Z/L \leq 0$. Following Loubet et al. (2001), to ensure **Eq. (S4)** exists, the source height is
65 taken as $Z_s = 1.01 z_0$. FIDES is essentially the same model as the one reported by Kormann and Meixner (2001).
66 The only difference resides in the way a , b , p and n are determined: in Kormann and Meixner (2001) these
67 constants are determined by equating U and K_z from Monin-Obukhov similarity theory to **Eqns. (S2 and S3)** at
68 the reference height (H), while in FIDES a range of heights ($2 \times z_0$ to 20 m) is used to compute these values.
69

70 | However, Wilson (2015) shows that under neutral stratification, any choice of $H/z_0 \gg 10$ should return an
71 | adequate concentration profile near the surface at fetches $1 \ll x/z_0 \ll 10^5$, hence FIDES and Korman and
72 | Meixner models can be considered equivalent in the range of dimensions considered in this study.

73 | **S4. Insuring coherency between WindTrax and Philip (1959) models (tuning FIDES with WindTrax)**

74 | **S4.1. Insuring comparable Schmidt numbers**

75 | The WindTrax software combines the backward Lagrangian stochastic (bLS) dispersion model described by
76 | (Flesch et al., 2004) with an interface where sources and sensors can be mapped. The transfer function $D(x_i, S_j, t)$
77 | is calculated by releasing N trajectories upwind from each sensor location x_i for each time step and recording the
78 | vertical velocity (w_0) of those that intersect the ground (N_{source} , or “touchdowns”). The transfer function is
79 | computed as:

$$81 \quad D(x_i, S_j, t) = \frac{1}{N} \sum_{N_{source}} \left| \frac{2}{w_0} \right| \quad (S5)$$

82 |
83 | In practice $N = 50000$ trajectories were used to compute D_{ij} . In WindTrax the Schmidt number (Sc , see
84 | 2.2) tends to 0.64 in the neutral limit as discussed by Wilson (2015).

85 | **S4.2. Insuring comparable Schmidt numbers**

86 | Most bLS models, and especially WindTrax assume $Sc = 0.64$, while models based on the eddy diffusion
87 | analogy, and hence FIDES and the Korman and Meixner model, lead to a Sc which was calculated in Carozzi et
88 | al. (2013) to be:

$$90 \quad Sc = \frac{u_*^2}{abp} Z^{1-p-n} \quad (S6)$$

91 |
92 | Hence constitutively, the Philip (1959) model does not lead to a constant Schmidt number in the surface layer,
93 | unless $1 - p - n \sim 0$, which was found to be the case under near neutral conditions (Carozzi et al., 2013). Note
94 | that the Korman and Meixner approach lead to $Sc = 1$ at the reference height in all conditions by construction.
95 | Furthermore, the stability correction functions are different in the Philip (1959) model and in WindTrax. Hence
96 | in order to compare the two approaches, the vertical diffusivity $K_z(Z)$ in FIDES was set as to reproduce the far
97 | field diffusivity of Flesch et al. (1995). Indeed, in bLS, the far-field diffusivity is $K_z = \sigma_w T_L$, where σ_w is the
98 | standard deviation of the vertical component of the air velocity, and T_L is the Lagrangian time scale. Replacing
99 | by their expression as in Flesch et al. (1995), leads to the following far-field diffusivity:

$$101 \quad K_z(Z) = 0.5\sqrt{1.7}u_*Z / \left(1 + 5\frac{Z}{L}\right) \quad \text{for } L > 0 \quad (S7)$$

$$102 \quad K_z(Z) = 0.5\sqrt{2.2}u_*Z \times \left(1 - 6\frac{Z}{L}\right)^{0.25} \left(1 - 3.3\frac{Z}{L}\right)^{\left(\frac{0.67}{2}\right)} \quad \text{for } L \leq 0 \quad (S8)$$

103

104 It is noticeable that in **Eqns. (S5 and S6)** there is a step change between stable and unstable conditions. Indeed,
105 when $L \rightarrow +\infty$ $K_z(Z) \rightarrow ku_*Z \times 0.63^{-1}$, while when $L \rightarrow -\infty$ $K_z(Z) \rightarrow ku_*Z \times 0.55^{-1}$. This means that in
106 WindTrax, the Sc number is set to 0.63 under stable conditions and 0.55 under unstable conditions and that in
107 near-neutral conditions Sc steps from 0.63 to 0.55 when passing from $L > 0$ to $L \leq 0$.

108 In FIDES, to ensure compatibility **with Flesch et al. (1995)**, Sc was set to 0.64 and parameters b/Sc and n
109 where adjusted so that $K_z(Z)$ in **Eq. (S3)** fits that in **Eqns. (S7 and S8)** over a logarithmically spaced vector of 30
110 heights from $z_0 \times 1.01$ to 2 m. **We should stress here that the expressions from Flesch et al. (1995) are slightly**
111 **different from those in Windtrax (Flesch et al., 2004):**

112

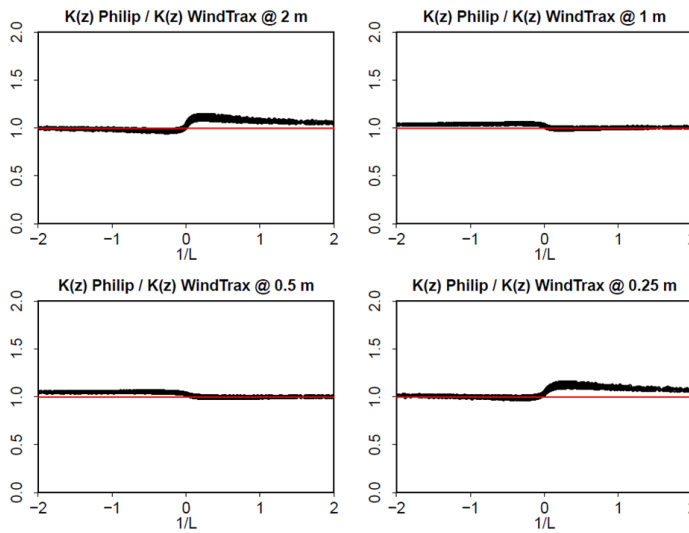
$$113 \quad K_z(Z) = 0.5 \times 1.25 \times u_* Z / \left(1 + 5 \frac{Z}{L}\right) \quad \text{for } L > 0 \quad (\text{S9})$$

$$114 \quad K_z(Z) = 0.5 \times 1.25 \times u_* Z \times \left(1 - 6 \frac{Z}{L}\right)^{0.25} \left(1 - 3 \frac{Z}{L}\right)^{1/3} \quad \text{for } L \leq 0 \quad (\text{S10})$$

115

116 **From the Eqns. (S9 and S10) is noticeable that under near neutral situations ($L \rightarrow +\infty$ or $L \rightarrow -\infty$), the**
117 **diffusivity $K_z(Z)$ is converges to $ku_*Z \times 0.64^{-1}$ (where $k = 0.41$ is the von Karman's constant and 0.64**
118 **represents the Schmidt number) and is continuous for all L . **Figure S1 based on Eqns. (S9 and S10) shows**
119 that our approach insures a coherency between the diffusivity of the bLS and Philip approach but small
120 differences remain which are height dependent. We should also notice that lateral dispersion was treated
121 separately in the two models, which will also lead to differences in the modelled concentration, especially for
122 larger fields.**

123

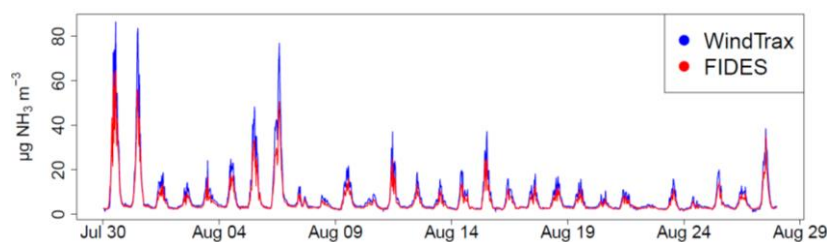


124
125 **Figure S1. Ratio of the “tuned” FIDES (“Philip”) to WindTrax vertical diffusivity for scalars ($K_z(z)$) as a function of**
126 **the inverse of Obukhov length (L/L) at 0.25, 0.5, 1 and 2 m heights. The tuned diffusivity corresponds to **Eqns. (S9**
127 **and S10).****

128

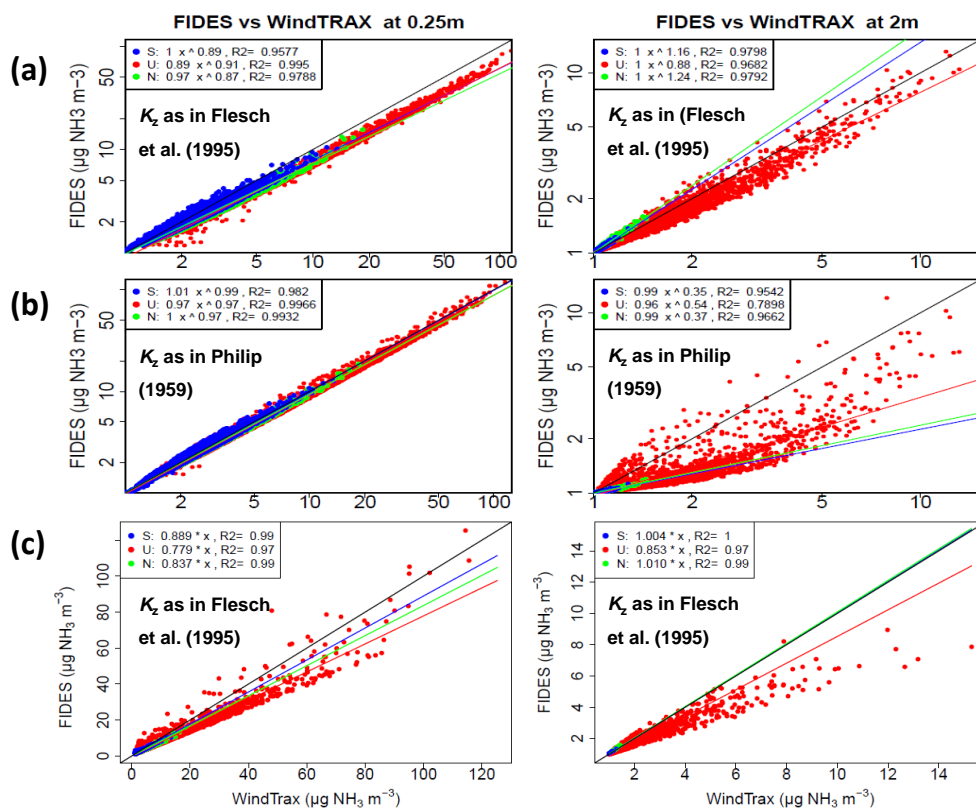
129 **S4.3. Comparison of FIDES and WindTrax models for predicting concentrations above a single source**

130 A first step in the study was to compare the two dispersion models. **Figure S2** shows that the “tuned” FIDES
131 model leads to the same concentration pattern as WindTrax **at 0.5 m above the source**, although systematically
132 underestimating the maximum concentration under unstable conditions. **This behaviour is clearly visible in**
133 **Figure S3 where the concentrations modelled with the “tuned” FIDES at 2 m above the surface (right**
134 **graph) are underrated by about 15% for unstable conditions compared to WindTrax, while matching for**
135 **stable and neutral conditions. We** further see that the concentration modelled with the original FIDES (Philip,
136 1959) are similar at 25 cm above the surface (left graphs) but differ substantially at 2 m above the surface (right
137 graphs). This is expected as the longer the travel distance, the larger the expected difference in dilution if the two
138 models’ diffusivity differ. In the original FIDES, the diffusivity is lower than in WindTrax by a factor of roughly
139 **one and half** ($Sc^{Philip} = 1$ and $Sc^{WT} = 0.64$). In a first order approach (over an infinitely homogeneous source), the
140 concentration difference between z_0 and 2 m would be proportional to the aerodynamic resistance (itself
141 proportional to the inverse of the vertical diffusivity) times the height above ground (see e.g. Flechard et al.,
142 2013), which explains the differences observed in **Figure S3**.



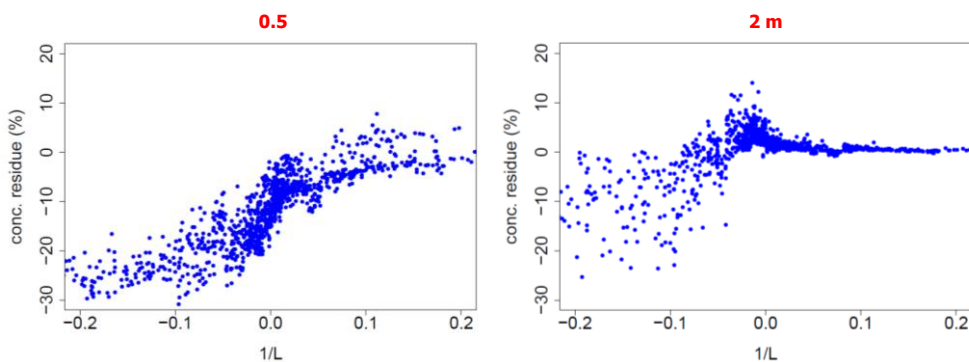
145
146 **Figure S2. Example concentration modelled above a single ammonia source using two dispersion models WindTrax**
147 **and FIDES with K_z as in Philip (1959), at 0.5 m above a simulated squared ammonia source of 25 by 25 m in the FR-**
148 **Gri ICOS site during August 2008.**

149



150
 151 **Figure S3. FIDES versus WindTrax concentration modelled above an ammonia source of 25 × 25 m at 0.25 and 2 m**
 152 **heights. In these graphs the FIDES vertical diffusivity K_z is either as in Philip (1959) (b) or fitted to Flesch et al. (1995)**
 153 **(a) and (c) as explained in S4.2. The comparison is made over the entire year of 2008 in the FR-Gri ICOS site. S, U**
 154 **and N stand for stable, unstable and neutral atmospheric conditions. The linear regression equation is given for each**
 155 **condition together with the R^2 of that regression. The black line is the 1:1 line. (a) and (b) show log-log axes an power**
 156 **law fits while (c) shows linear axes and linear fits.**

157 **Figure S3** also shows that the “tuned” FIDES modelled concentrations (top graphs) do not perfectly fit to the
 158 **WindTrax** ones (top graphs in **Figure S3**). At height of 25 cm, the “tuned” FIDES concentration does lead to a
 159 worse regression score than the original FIDES. Although **Figure S3** is focussing on a 25 m × 25 m field, the
 160 results are similar for larger fields (data not shown). This is explained by the difference in Z -dependency of K_z
 161 in the WindTrax and FIDES model, which is highlighted in **Figure S1**: under stable conditions ($1/L > 0$), “tuned”
 162 FIDES $K_z(Z)$ is larger than WindTrax at 0.25 and 2 m, but smaller at 0.5 and 1 m, and the opposite under
 163 unstable conditions ($1/L < 0$). This means that constitutively the two models may never fit perfectly, showing a
 164 bias that will depend on height. Nevertheless, the correlation between the two models is very high as shown by
 165 large $R^2 \geq \sim 0.96$.



166
167

168 **Figure S4. Relative difference between FIDES and WindTrax concentrations as a function of the stability parameter**
169 **($1/L$). Data refer to the same conditions reported in Figure S3.**

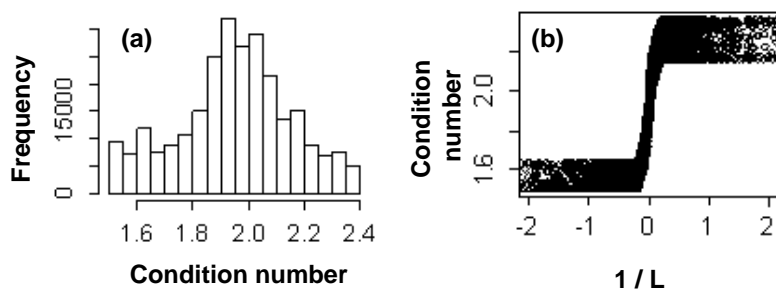
170

171 **Figure S4 reports the relative difference between the NH_3 concentration calculated by the two models at**
172 **0.5 and 2 m height, as a function of the stability parameter ($1/L$). As previously stated, under unstable**
173 **conditions FIDES clearly underestimates the concentrations up to 30% at 0.5 m and lower heights, while**
174 **this gap is reduced and more scattered at 2 m height. Moving towards neutral conditions the two models**
175 **tends to agree notwithstanding an overestimation to 10% by WindTrax at 2 m height concurrently with**
176 **an underestimation of the same magnitude by FIDES at 0.5 m. Under stable conditions there is a clear**
177 **agreement at 2 m height, while this correspondence remains unbalanced to lower heights.**

178

179 **Supplementary figures**

180



181

182 **Figure S5. (a) Distribution of condition numbers for the 0.25 m height sensor and the 25 m width plots, for integration**
183 **periods of 6h and 24h, and (b) condition number as a function of $1/L$, where L is the Obukhov length.**

184

185 **References quoted in the supplementary material**

- 186 Carozzi, M., Loubet, B., Acutis, M., Rana, G. and Ferrara, R.M., 2013. Inverse dispersion modelling highlights
187 the efficiency of slurry injection to reduce ammonia losses by agriculture in the Po Valley (Italy).
188 *Agric. For. Meteorol.*, 171: 306-318.
- 189 Crenna, B.R., Flesch, T.K. and Wilson, J.D., 2008. Influence of source-sensor geometry on multi-source
190 emission rate estimates. *Atmos. Environ.*, 42(32): 7373-7383.
- 191 Flechard, C.R. et al., 2013. Advances in understanding, models and parameterizations of biosphere-atmosphere
192 ammonia exchange. *Biogeosciences*, 10(7): 5183-5225.
- 193 Flesch, T.K., Harper, L.A., Desjardins, R.L., Gao, Z.L. and Crenna, B.P., 2009. Multi-Source Emission
194 Determination Using an Inverse-Dispersion Technique. *Boundary-Layer Meteorology*, 132(1): 11-30.
- 195 Flesch, T.K., Wilson, J.D., Harper, L.A., Crenna, B.P. and Sharpe, R.R., 2004. Deducing ground-to-air
196 emissions from observed trace gas concentrations: A field trial. *J. Appl. Meteorol.*, 43(3): 487-502.
- 197 Flesch, T.K., Wilson, J.D. and Yee, E., 1995. Backward-Time Lagrangian Stochastic Dispersion Models and
198 Their Application to Estimate Gaseous Emissions. *J. Appl. Meteorol.*, 34(6): 1320-1332.
- 199 Gao, Z.L., Desjardins, R.L., van Haarlem, R.P. and Flesch, T.K., 2008. Estimating Gas Emissions from Multiple
200 Sources Using a Backward Lagrangian Stochastic Model. *Journal of the Air & Waste Management*
201 *Association*, 58(11): 1415-1421.
- 202 Kaimal, J.C. and Finnigan, J.J., 1994. *Atmospheric Boundary Layer Flows, Their structure and measurement.*
203 Oxford University Press., New York, 289 pp.
- 204 Kormann, R. and Meixner, F.X., 2001. An analytical footprint model for non-neutral stratification. *Boundary*
205 *Layer Meteorol.*, 99(2): 207-224.
- 206 Loubet, B., Milford, C., Sutton, M.A. and Cellier, P., 2001. Investigation of the interaction between sources and
207 sinks of atmospheric ammonia in an upland landscape using a simplified dispersion-exchange model. *J.*
208 *Geophys. Res.-Atmos.*, 106(D20): 24183-24195.
- 209 Philip, J.R., 1959. The Theory of Local Advection .1. *J Meteorol.*, 16(5): 535-547.
- 210 Sutton, O.G., 1932. A Theory of Eddy Diffusion in the Atmosphere. *Proceedings of the Royal Society of*
211 *London. Series A*, 135(826): 143-165.
- 212 Wilson, J.D., 2015. Computing the Flux Footprint. *Boundary Layer Meteorol.*, 156(1): 1-14.
- 213

bg-2017-424-RC1: answer to referee 1 comments.

We would like to thank referee 1 for his helpful comments which we have answered below.

General Comments

This study carried out are providing answers to the much discussed question about the effect of having many plots in the field on measured ammonia emission from manure applied on the plots. Exploring the effect of measuring average ammonia concentration for increasing time intervals, the numbers of measuring heights and the best heights for measuring the emission. The answers to these questions are most important and the issue is discussed by scientist in Europe especially after the publications of Sinterman et al. questioned the existing design of measuring ammonia emission

The authors have developed a model for calculating emission of ammonia from as it varies over the day and year as affected by surface soil temperature, wind and atmospheric stability. Then, as I understand the paper, they calculate how much the emitted ammonia will contribute to atmospheric ammonia concentration at different heights above the soil surface as it is affected by climate and plot size i.e. the loss pattern over time after volatilization start is assessed using decay curves of source strength.

The atmospheric NH₃ concentration data, climate data are then used as input to model calculation of the emission from a plot and plots in a field as affected a range of different management of measuring ammonia concentration, height of the ammonia concentration measurements, number of plots affecting ammonia concentration in plots downwind a plot, plot size, etc.

This reviewer is not a specialist in micrometeorology so I cannot evaluate the quality of the model calculations. In the following is my impression of the presentation and interpretation of the data.

Abstract

Line 9 NH₃ is presented but later the authors write ammonia – should be NH₃

This is a sound remark; we agree that we can use NH₃ throughout the manuscript once it has been defined as “tropospheric ammonia” except when it is the first word of a sentence.

Line 10: the abbreviation N for nitrogen should be given and N used in the text.

We thank the referee for the suggestion; we however think we could stick with “nitrogen” to avoid too many abbreviations in the abstract.

I am not familiar with the term inference method, the term inferring, inferred in this context? May be because my native language is not English.

We agree with the referee that “to infer” may not be a very commonly used term. It is a synonym of “to deduce”. We hence speak about a “source inference method” in the sense that the method is used to “deduce” the ammonia source.

L68: What is an intensive source?

We thank the reviewer for spotting this term which we might have mis-used. We rather wanted to mean an intense or strong source. We propose to change term the “intensive” to “strong” in the manuscript.

L69-70: require hourly concentrations of what???

Of NH₃. We propose to add this precision in the text.

L87 Multiple-source inversion problem?

We thank the reviewer for spotting this incoherency. Actually, we defined what we meant in lines 76-77, as “the multiple source problem, which consists of inferring multiple sources based on measured concentrations at multiple points in space and time,...”. We hence propose to use the term “multiple-source inference problem” throughout the manuscript to keep it coherent.

L121-124: Units are missing

Thanks for spotting that the units for concentration and emissions were missing. The concentration and source are in $\mu\text{g N-NH}_3 \text{ m}^{-3}$ and $\mu\text{g N-NH}_3 \text{ m}^{-2} \text{ s}^{-1}$, respectively. We propose to add these precision in the manuscript.

L324-327: Has the data from this experiment been used in previous articles, reports, proceedings?

Results from this experiment have been used jointly with other experimental trials in a poster proceeding, but not for testing the multiple-source inference methodology presented here. The poster was presented at a French meeting on fertilisation. The objective was to compare the emissions potential from several treatments based on the use of a “gradient” method applied to badges. The objective of the poster presentation was to show the potential of using alpha badges to differentiate nitrogen application methods in terms of potential ammonia losses. The link to the poster abstract in French is here:

http://www.comifer.asso.fr/images/pdf/11emes_rencontres/Interventions/Session%201/5%20-%20Jean-Pierre%20COHAN/Article%20Jean-Pierre%20COHAN.pdf.

L355-356: Rewrite

We propose to change to the following simplified sentence: “The friction velocity u^* varied between 0.024 and 1.181 m s⁻¹, and the stability parameter z/L varied between -49 and 21 m⁻¹ (Figure 3).”

383: Condition number – what is this – referring to an equation S1 in annex, it is a number often used so a presentation of how it is calculated should be given in the article

The condition number is indeed an important indicator of the geometry of the multiple sources inference problem. We feel that it was well defined and discussed in the supplementary material section S2. The way it is calculated in practice is mentioned at line 46 of the supplementary material. We propose to slightly modify this sentence to make it even clearer: “In practice, the calculation of CN was performed using the kappa function in R (version 3.2.3).” We also propose to add the phrase “(see supplementary material section S2)” to lines 384 and 684 of the manuscript where this indicator is mentioned.

P519: When discussing the effect of height for measuring the horizontal then the authors should relate the outcome of their study to that of Wilson et al. who showed on basis of micro-met. Calculations that there is a best height for measuring the horizontal flux at one height (This Zinst height is higher than the height recommended here)

Although the ZINST method has no link with our approach, it is an interesting remark that brought back to our attention that the heights at which the alpha badges should be placed would depend on roughness length and displacement height. Indeed, the ZINST method is a method that uses the finding of Wilson et al. (1982) that the ratio of the source strength to the horizontal flux at height ZINST is somewhat constant whatever the stability conditions. Interestingly, Wilson et al. showed that ZINST was an exponential function of z_0 for a given source diameter. We hence propose to add the following text after Line 519: “It is interesting to note that the height which was found to provide an optimal inference of NH₃ sources (below 0.5 m) is smaller than the ZINST reported by Wilson et al. (1982) (which was 0.9 m for 40 m diameter circular sources, and which we estimate as 0.65 m based on a power law extrapolation as in Laubach et al. (2012)). It is also important to note that this height should vary with both the roughness length z_0 and displacement height as was showed by Wilson et al. (1982) for ZINST.”

L555: What is the highest source?

We actually meant the largest source. We propose to change the text in L555 and L540 and also Figure 12 accordingly.

Figures:

The font size of the Y and X axis and some of the legends are too small on most figures. On some figures there are too many lines (7 lines on fig 4) making it very difficult to see the individual lines.

We thank the reviewer for his suggestion. We have looked at the figures thoroughly again and we agree indeed that some figures may be difficult to read, but most figures look good to us. We propose to improve some figures as explained below but we would like to have the editor's point of view for the other figures.

- Figure 4: we propose to reduce the number of integration periods and to keep only 0.5h, 24h and 168h which are sufficient to show the variability that is lost by integrating concentration measurements.

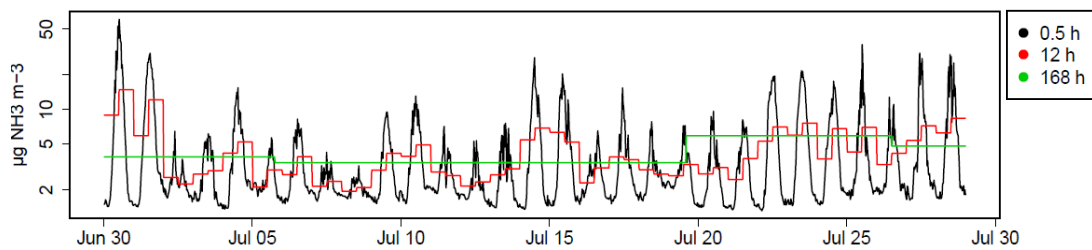


Figure 4. Example modelled concentration pattern at 1 m above a single 50 m width source for several averaging periods (0.5h, 12h and 168h) for the month of July 2008. The source Γ was set to 10^5 . The y-axis is log scaled.

- Figures 5: there were some legends that we left in the right corner but these are not useful as the main legend was written at the top of the graph. We propose to erase these legends:

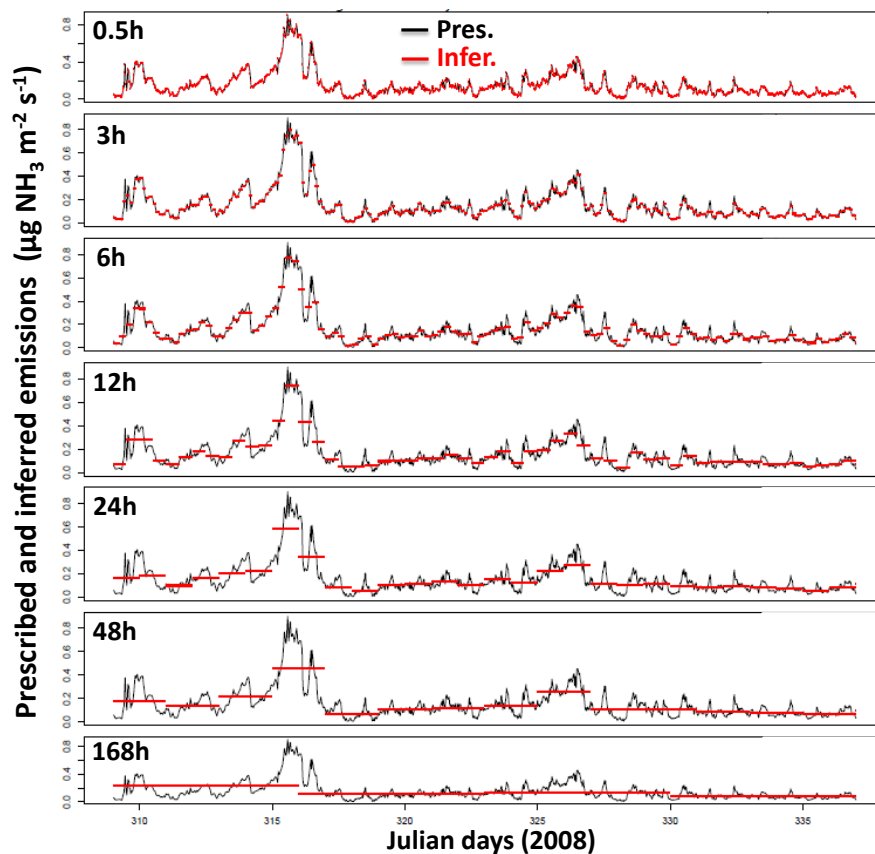


Figure 5. Example source inference for a 25 m width square field and a concentration sensor placed at 0.5 m above ground. Here $\Gamma = 10000$ and is set to constant (pattern 1). The 7 integration periods are shown: 0.5h to 168h. The x-axis shows the day of year and corresponds to a span over November. The prescribed source is in black (Obs.) and the inferred one in red (Pred.)

- Figure 7: we propose to change the font size and the Y axis label. We will also change the caption for u_* and $1/L$ classes:

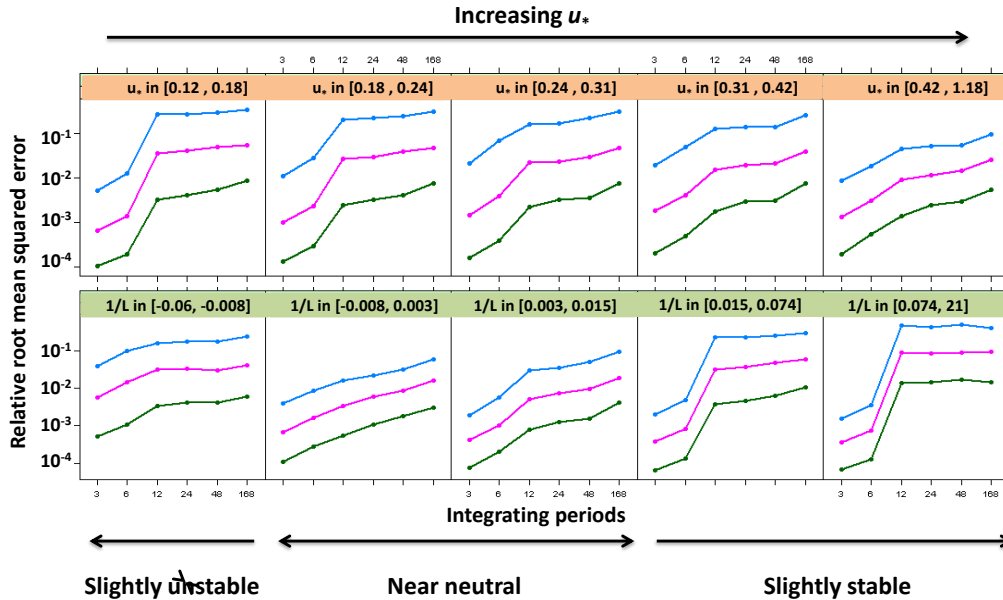


Figure 7. Relative root mean squared error as a function of integration period for stability factor and friction velocity classes for a single 25 m side field. Medians and quartiles are given for equally sized bins of u_* and $1/L$ and for the lowest sensor height (0.25 m). The blue, pink and green curves are the 3rd, 2nd and 1st quartiles, respectively.

Figure 5 & 8: I assume that prescribed is the emission data provided by calculation and inferred is emission calculated by knowing NH3 concentration at 0.5 m and weather conditions.

Indeed prescribed emissions are calculated using equations (9) and (10) with a constant Gamma, and inferred are those based on measured concentration at 0.5 m height and transfer coefficient using equation (7).

Fig. 7: Need improvement

We agree. See previous section for our proposition.

Fig 9; Why not mention the emission strength of the source instead of Treatment 1-3 (what is the units?)

This is indeed a sound remark. We propose indeed to use the emission potential Γ , which actually has no units. Figure 9 would look like this (Figures 10-12 would be changed accordingly):

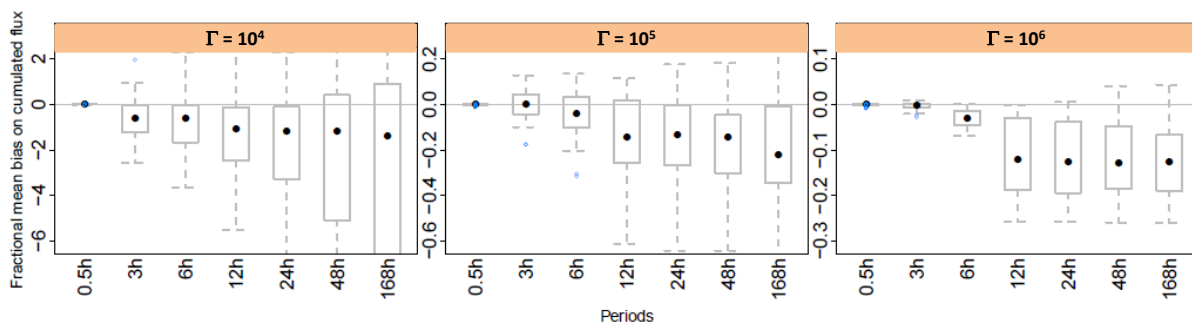


Figure 9. Effect of integration period on source inference in the multiple-plot setup. The fractional mean bias of the source is shown for each treatment. Inference strategy C1 was used (single sensor, independent blocks, and background concentration known). Statistics for runs with target heights 0.25 and 0.5 m and source side = 25 m are calculated. All application periods are considered. Filled points show medians, boxes show interquartiles and bars show minimums and maximums. Outliers are points to 1.5 times away from boxes limits.

Fig 16: Is it correct that measured emissions are not included – if so then the measured results should be included?

There might be a misunderstanding of that figure; indeed Figure 16 reports inferred emissions using the multiple-source inference method that was presented and discussed in this manuscript. But in that experiment no other method than this one was used to “measure” emissions. This is actually our point to show that this inference method is appropriate for estimating the emissions under real situations. In a way our inference method gives a measurement of the ammonia emissions.

References quoted in the answer to reviewer 1

- Laubach, J., Taghizadeh-Toosi, A., Sherlock, R.R. and Kelliher, F.M., 2012. Measuring and modelling ammonia emissions from a regular pattern of cattle urine patches. *Agric. For. Meteorol.*, 156: 1-17.
- Wilson, J.D., Thurtell, G.W., Kidd, G.E. and Beauchamp, E.G., 1982. Estimation of the rate of gaseous mass transfer from a surface source plot to the atmosphere. *Atmospheric Environment* (1967), 16(8): 1861-1867.

Answer to Referee 2 comments

We thank Referee 2 comments which we hope will help us improving our manuscript.

General Comments

Loubet and others study a new method for inferring ammonia loss from small agricultural plots. I found the modelling analysis to make for an interesting case study regarding the applicability of field experiments. The approach treats bias errors carefully. As a consequence, I feel that the manuscript makes an earnest effort to quantify biases associated with passive ammonia sampling over small agronomic field plots and will be a valuable contribution to the literature.

Minor comments:

‘Further work should anyway be produced for validating this method in real conditions’ at the end of the abstract does not sound hopeful. Rather, the authors should try to discuss strategies for further improving the method and reducing uncertainties.

We thank the reviewer for this comment. We have indeed identified two strategies for further improving the method: (1) using Bayesian inference which has the potential for constraining the emissions and avoiding unrealistic sources inference as shown by Yee and Flesch (2010), and (2) changing the cost function (also called objective function); instead of inferring the emission strength, we could infer the emission potential Γ (a strictly positive number). This last method has the advantage of avoiding non-plausible deposition fluxes, because the flux is calculated as the concentration above the source minus the concentration at the ground, divided by transfer resistance. With such an approach negative fluxes (deposition) can occur within the limit of plausible transfer resistances but not above. We believe that the combination of these two strategies has the potential to improve the method substantially.

We think that “calibration” of the method against controlled sources is a remaining challenge that needs to be tackled (as also suggested by the comments of A. Neftel and C. Hanni in the interactive discussion).

We hence propose to add this more positive statement at the end of the abstract: “We believe that the method could be further improved by using Bayesian inference and inferring surface concentrations rather than surface fluxes. Validating against controlled sources is also a remaining challenge.”

Line 41: 55.3% sounds remarkably specific given uncertainties in measuring NH₃ flux.

This is a sound comment. We propose to change to 55%.

53: ‘most of the time large fields’ is awkward wording.

Indeed. We propose to change to “most of the time also requires the use of large fields”

57: agronomic trials are not necessarily of those dimensions.

This is a sound remark indeed and we should not be as general as we were. We would propose to change to: “Especially useful for measuring ammonia losses are methods that can deal with small and medium-scale fields (20-50 m on the side) that are commonly used in agronomic trials.”

Parentheses on line 67.

Thanks for spotting this. We have withdrawn the left parenthesis.

118: quotes are unnecessary.

We agree and have withdrawn them.

On 130, what is the typical reaction time (and thereby Damkoehler number?)

Typical Damköhler numbers showed by Nemitz et al. (2009) above a cut grassland canopy fertilised with ammonium nitrate were from 0.001 to 1. Values greater than 0.1 only occurred marginally, and usually during night-time conditions (Figure 6 in Nemitz et al. 2009). We would of course expect larger Damköhler number values for slurry application which may generate larger concentrations than those reported by Nemitz et al. (2009), or with surface canopies having larger residence times. But in any case we expect the chemical depletion of ammonia to remain small at the spatial scale we are focussing on (around 200-300 m).

I find the tau near the overbar in 2 and other equations to be a bit distracting because it could be confused with an exponential term.

This is a sound remark. We propose to remove the *taus* and just leave an explanation in the text that the overbars denote averages over the period tau.

Equation 4 could be rearranged to reflect that only the numerator of the second term on the right hand side is unknown.

It is true that the numerator of the second term is the only unknown. However we can't see how to isolate this term apart from multiplying by $D(x)$. Moreover, leaving the equation as it is now has the advantage of explicitly showing this term which is the bias. We hence propose to keep equation (4) as it is.

251: why is z_{ref} 3.17 m? The curly braces in $R_b\{NH_3\}$ I find to be a bit distracting.

Regarding z_{ref} , we subjectively choose to use the reference height z_{ref} as the height where our ultrasonic anemometer was placed in the field, which simplified the calculation of the aerodynamic resistance for us. This does not have much importance anyway as we assumed that atmospheric ammonia concentration was zero.

Regarding R_b , we propose to change $R_b\{NH_3\}$ to R_{bNH_3} .

263: is there a justification for the model in simulation 2?

Exponential decrease in emission potential is representative of strong NH_3 emissions like those happening following slurry application. The value of 4.6 and the time scale τ_0 were chosen arbitrarily and would represent emissions a little bit less intense than those for nitrogen applications reviewed by Massad et al. (2010). In fact the equation we used here would be equivalent to a time scale equal to 6 days while in Massad et al. (2010) they report a time scale of 2.88 as being representative of slurry application. We propose to add the following text in Line 270: "The time scale of the exponential decrease we used here was around 6 days, which is twice as large as the one reported by Massad et al. (2010) for slurry application (2.9 days)."

265: what are typical parameters for the Gaussian model? Also, what mechanism causes it? The urea spreader?

The Gaussian model is rather representative of urea application. Indeed, NH_3 emissions result from combined processes: first the urea is hydrolysed by urease enzymes which release ammonium which can be volatilised but can also be nitrified or absorbed by roots. This leads to typical emissions starting a few days following application and showing a maximum up to 15 days following application but also a slower decrease of the emissions following the peak.

The Gaussian model was centred on day 14 with a standard deviation of 8.4 days.

267: I understand why 4.6 now in simulation 2. . .but why does this 'best' represent NH_3 emissions?

As explained in previous paragraphs and following Massad et al. (2010) this model best represents slurry applications.

302: why is the covariance term negligible at the half hourly period? The spectral gap in eddy covariance studies?

The covariance term is indeed negligible at that time scale because of the so-called spectral gap in eddy covariance studies. This gap corresponds to time scales at which there is little energy in the

turbulence and surface flux spectra (see e.g. Van der Hoven {, 1957 #25437}). We propose to replace the sentence at line 302 by “In practice the concentrations were computed at each sensor location using Eq. (6) over 0.5h: at that time scale, which corresponds to the spectral-gap, the covariance term is assumed to be negligible (Van der Hoven, 1957).”

303: in 2.5.3, these are not hypotheses as they cannot be falsified, even in the model.

This is indeed an interesting remark. We propose to change to the term “scenario” instead.

327: extra point

Thanks for spotting this. We have removed it.

336: how close is ‘nearby’? From the figure it looks like it was part of the larger setup.

The meteorological data were measured at around 25 m away from the edge of the central plots (Figure 2). We propose to change the sentence for clarification: “The meteorological data were measured at less than 50 m from the central plots (Figure 2)”.

355: results should be written in the past tense.

Thanks for the comment. We propose to change this sentence also to clarify its meaning : “The friction velocity u^* varied between 0.024 and 1.181 m s⁻¹, and the stability parameter z/L varied between -49 and 21 m⁻¹ (Figure 3)”

365: define Gamma for the reader in the figure legend.

Thanks for the comment. We propose to change the last part of the legend to “...with an emission potential $\Gamma = 10000$ ”

Please avoid using red and green simultaneously in Figure 4. This figure appears to be made using R, and gray is also a default color. And honestly yellow is never a good choice on a white background.

The comment that Figure 4 was hard to read was also made by reviewer 1. We have hence simplified the Figure and we further propose to change the colors as suggested by reviewer 2:

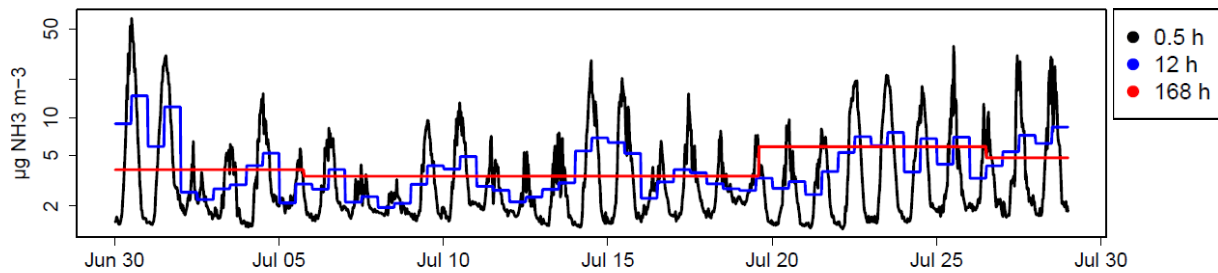


Figure 4. Example modelled concentration pattern at 1 m above a single 50 m width source for several averaging periods (0.5h, 12h and 168h) for the month of July 2008. The source Γ was set to 10^5 . The y-axis is log scaled.

384: focuses

Thanks for spotting this typo. We have corrected it.

Figure 6 confuses me a bit because the 13 periods vary so strongly in their meteorological conditions from summer to winter, why are they grouped? The bars also leave the figure in the upper left subplot.

The idea for grouping the periods in Figure 6 but also in Figures 9-11 and 14 is actually to evaluate the variability of the bias due to meteorological conditions: ideally, if the method shows little variability in the bias, this bias could be characterised and even withdrawn. In Figure 6 we try to give a broad view of how the bias changes with sensor height and plot width. Figure 7 actually shows the variability of the bias due to meteorological conditions.

Regarding the scale, we chose to have a single scale for all panels to ease the comparison between heights and plot size, and we also chose to get the scale focussed enough to better see biases in the range -0.2 to 0.1. What we conclude from the upper left subplot is that the bias is much larger than all other cases which shows that that combination height-plot size is not satisfactory.

464-466: the attribution of stability with respect to continental vs. oceanic sites is too much of an approximation. There are many continental sites that are consistently windy, often due to orography.

We agree that we might have been too approximate in this statement, although we might still agree on the fact that oceanic conditions are typically windy. We propose to withdraw the reference to continental or oceanic climate to make it more general and replace the sentence for the following one: "We conclude that the inference method with a long integration period will lead to very moderate biases for locations with near-neutral conditions and high wind speed, but may lead to much larger bias under stable conditions and low wind speed as soon as the integration period gets up to 12 hours."

There is a strange x on line 468. Font sizes for figure 7 should be increased.

Thanks for spotting the x. It came from a problem when pasting Figure 7. We propose to modify Figure 7 to increase font size and improve as follows:

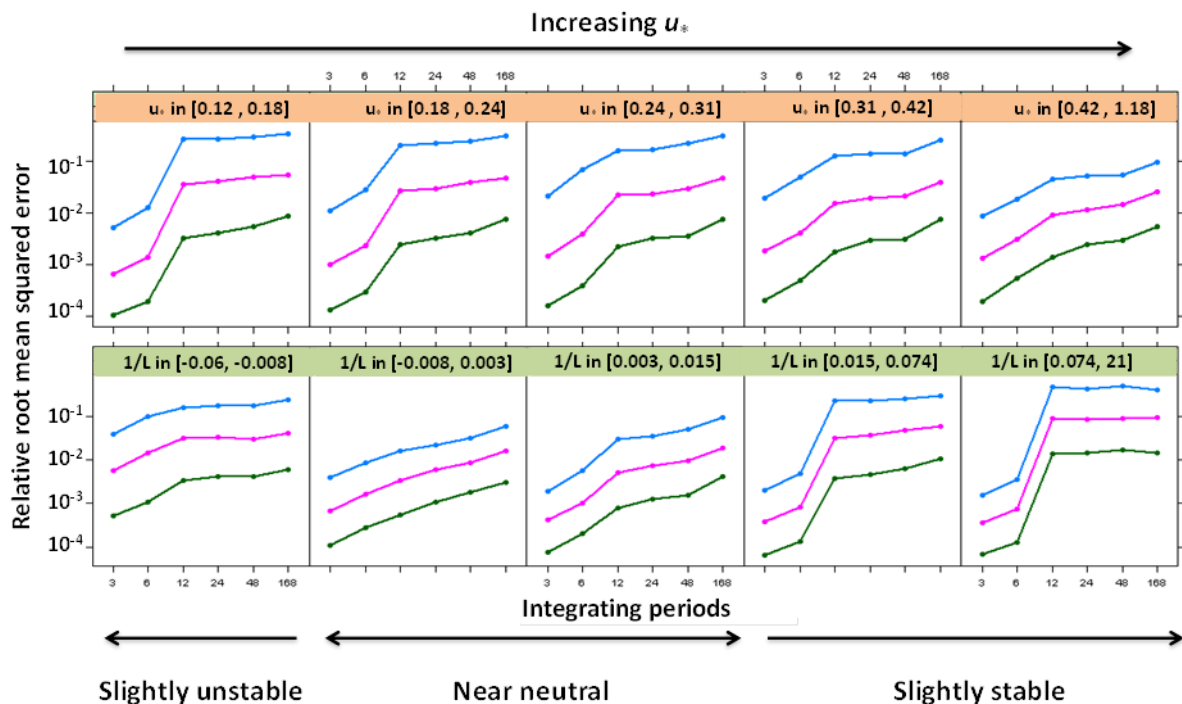


Figure 7. Relative root mean squared error as a function of integration period for stability factor and friction velocity classes for a single 25 m side field. Medians and quartiles are given for equally sized bins of u_* and $1/L$ and for the lowest sensor height (0.25 m). The blue, pink and green curves are the 3rd, 2nd and 1st quartiles, respectively.

741: why bird colonies?

Actually the only references we found where this bias was evaluated were those from emission estimates from bird colonies. We propose to withdraw the mention to bird colonies as this does not add much to the conclusion statement.

742: again, continental does not imply low wind speeds.

As in previous comment we propose to withdraw the reference to continental climate.

References

- Massad, R.S., Nemitz, E. and Sutton, M.A., 2010. Review and parameterisation of bi-directional ammonia exchange between vegetation and the atmosphere. *Atmospheric Chemistry and Physics*, 10(21): 10359-10386.
- Nemitz, E. et al., 2009. Aerosol fluxes and particle growth above managed grassland. *Biogeosciences*, 6(8): 1627-1645.
- Yee, E. and Flesch, T.K., 2010. Inference of emission rates from multiple sources using Bayesian probability theory. *J. Environ. Monit.*, 12(3): 622-634.

Answer to Comment to the paper „Evaluation of a new inference method for estimating ammonia volatilisation from multiple agronomic plots “by Benjamin Loubet et al. by Albrecht Neftel (Neftel Research Expertise, CH-3033 Wohlen b. Bern, CH, Switzerland) and Christoph Häni (School of Agricultural, Forest and Food Sciences, Bern University of Applied Sciences, CH-3052, Zollikofen, CH, Switzerland)

This paper presents an appealing and low-cost approach to determine NH₃ losses from adjacent multiple agronomical plots by a combination of concentration measurements using passive sampler devices and a dispersion model that is driven by turbulent parameters inferred from standard 30 minutes meteorological data.

The aim of the paper is described as: “Can inverse dispersion modelling approaches be used for inferring NH₃ emissions from multiple small plots (agronomic trials) using passive samplers, and to which degree of accuracy?”

The overall answer is encouraging with the statement in the conclusions “In this study we have demonstrated that it is possible to infer with reasonable biases ammonia emissions from multiple small fields located near each other using a combination of a dispersion model and a set of passive diffusion sensors which integrate over a few hours to weekly periods”.

According to our judgement the accuracy will be mainly determined by two aspects addressed below.

a) Bias related to the applied dispersion modelling

Dispersion models are a simplified mathematical representation of the turbulent motion in the surface layer and will always deviate from reality. Systematic biases can be expected when modelling the lower heights of the measurements that are discussed in this paper. For concentration sensors placed close to the ground (e.g. 25cm above ground) **transfer functions are likely to be biased due to e.g. the needed simplifications that must be made to describe the exchange process at the ground, the natural heterogeneity on a small scale at the surface or the violation of model assumptions such as the failure of K-theory close to the canopy (Raupach and Legg, 1984). Furthermore, the translation of the sensor height in a model framework is challenging for very low heights since the sensor height value (and with that the resulting value of D at that location) becomes very sensitive to sensor height measurement errors as well as to the absolute values of z₀ and d. To us, a sensor height of 25 cm seems too close to the surfaces.**

We do agree with A. Neftel and C. Häni concern that model representations may be biased close to the ground, and especially Gaussian like models, since they do not intrinsically account for near-field dispersion as shown by Raupach and Legg (1984) and subsequent publications from M.R. Raupach (Raupach, 1987; Raupach, 1989b). This is not the case of the Langevin models that account for near-field dispersion (Raupach, 1989b; Thomson, 1987). However, as exposed by Raupach (1989a), the height at which the near-field effect is sensible would be equal to $\sigma_w T_L \sim 0.3 \sigma_w h / u_* \sim 0.3 \times 1.25 \times h \sim 0.4 h$ where σ_w is the vertical air velocity standard deviation, h is canopy height and T_L is the Lagrangian time scale. Numerical values were derived from Raupach (1989a), Figure 1. Hence we would expect this far field effect to be small on situations with small canopies (or by extension with

small roughness height for a bare soil). Typically this would correspond to about 5 cm above a 10 cm canopy and ~1 cm above a 3 cm roughness. Hence we agree with A. Neftel and C. Häni that this would represent a quite important fraction of the sensor height if this sensor would be placed lower than 50 cm (20% for 25 cm). This would especially be critical for canopies that are taller than 10 cm.

Regarding the uncertainty in determining the height of the sensor close to the ground, this is a very sound remark. We however see in Figures 6 and 10 of the manuscript that the method gives similar biases for sensors placed at 25 cm and 50 cm above ground (and also close biases for $h = 1$ m), for plots of 25 m x 25 m. We hence agree with the concern of A. Neftel and C. Häni that 25 cm would be too low and we should rather target heights of 50 cm. We propose to add this statement in the conclusions: *“Although the lowest sensors have the best condition number, we would rather recommend in practice using heights of 50 cm above the canopy in order to reduce uncertainty in positioning the sensors close to the ground as well as avoid being too close to the roughness layer close to the canopy which is characterised by non-diffusive transfer.”*

The authors are using their FIDES-3D model that is based on an analytical solution of the advection-diffusion equation. This model is compared with the backward Lagrangian Stochastic dispersion (bLS) model described in Flesch et al. (2004) (the “WindTrax” software, Thunder Beach Scientific, Nanaimo, Canada). For the presented analysis the FIDES model K_z was adopted to match the far field approximation of K_z of the bLS model. **We are missing an explanation, why this was done.**

The aim of matching the far-field diffusivity of the two models was to make the FIDES model consistent with the bLS approach, which is a commonly used method nowadays for estimating ammonia emissions with inversion techniques. As exposed in the manuscript, one major difference arises from the fact that the Phillip (1959) approximation of the advection-diffusion equation (which is identical to the approach of Korman and Meixner (2001)) has a Schmidt number equal to 1, while bLS approaches have a Schmidt number equal to 0.64. Wilson (2015) showed that the choice of the Schmidt number has a great effect on footprint, and hence on concentration above a small source and should therefore be explicitly given. Wilson further showed that the difference in footprints predicted by diffusion and Langevin models (like bLS) are small under neutral and stable conditions provided they have similar Schmidt numbers, although the difference in footprints remains large under unstable conditions even with identical Schmidt number (with the Langevin models diffusing less than the Eulerian ones). We hence chose to use an approach that was as close as possible to the bLS approach. To do so, we matched the far field diffusivities of the two models, as this would ensure that the two models would provide similar concentrations at heights larger than a few decimetres. Moreover there was no point in matching near-field dispersion, as FIDES does not account for near-field dispersion.

In the supplement, a detailed investigation is presented how the two models differ in their formulation of the vertical diffusivity K_z . The assumed far field vertical diffusivity in the bLS model is approximated by parametrizations provided in Flesch et al. (1995). We would like to remark that WindTrax uses slightly different default parametrizations of σ_w than provided in Flesch et al. (1995) (see e.g. the manual on the WindTrax homepage). This is resulting in vertical diffusivities given as:

$$Kz(Z) = 0.5 * 1.25 * u_* Z / (1 + 5Z/L) \text{ for } z/L \geq 0 \quad (\text{WT1})$$

$$Kz(Z) = 0.5 * 1.25 * u_* Z \times (1 - 6Z/L)^{0.25} (1 - 3Z/L)^{(1/3)} \text{ for } z/L < 0 \quad (\text{WT2})$$

with a Schmidt number value of $Sc \cong 0.64$ for near-neutral stabilities with a smooth transition from $L = \infty$ to $L = -\infty$. These equations differ from the equations S7 and S8, and imply a different interpretation of the differences between FIDES and WindTrax, though without changing the numeric results of the comparison.

We would like to thank C. Häni and A. Neftel for providing the exact expression used in Windtrax. We indeed only referred to the work of Flesch et al. (1995). These equations WT1 and WT2 are more consistent than those we reported since, as opposed to equations S7 and S8, they insure continuity in $Kz(Z)$ when $z/L \rightarrow 0$. We see from the set of equations WT1, WT2, S7 and S8 that $Kz(Z)$ is similar under non-neutral conditions in S7 and WT1 though 4% smaller in Windtrax but that $Kz(Z)$ is 16% smaller in Windtrax (WT2) than in the “tuned FIDES” (S8) under unstable conditions. This therefore explains better Figure S3 which shows a good fit between the “tuned FIDES” and WindTrax under stable and neutral conditions but a lower concentration modelled with the “tuned FIDES” at 2 m above ground under unstable conditions. Indeed, since the far-field diffusivity is larger in the tuned FIDES, this model lead to larger diffusion and hence lower concentrations away from the source. However, another difference comes from constitutive differences between Eulerian and Langevin models under unstable conditions as shown by Wilson (2015).

We have checked that the results reported in this manuscript remain mostly unchanged since already in line with the most important feature of $Sc \sim 0.64$. We however quantified a difference of around $-18\% \pm 10\%$ in the concentration modelled using equations S7 and S8 (Flesch et al., 1995) compared to equations WT1 and WT2 (Flesch et al., 2004) for a single source of 25 m x 25 m. Since this difference is systematic and since we use the same model for forward and backward modelling we do not expect any impact on the conclusions we have drawn from this study. Indeed, we checked for a single source of 25 m x 25 m that the biased inferred using eq. S7 and S8 and WT1 and WT2 were similar within less than 1% for most cases. Noticeably, the biases for the highest sensors were diminished with WT1 and WT2. We hence propose to leave equations s7 and S8 in section S4.2 as they are but to stipulate explicitly that these correspond to Flesch et al. (1995) and not to WindTrax. We also propose to modify Figure S3 to explicitly mention this (see new Figure 3 below).

In the supplement Figure S3 presents a comparison between evaluated concentrations with FIDES and WindTrax respectively using the prescribed emission sources with the SVAT model. This figure is hiding the apparent differences as a double logarithmic representation is used and the concentrations are shown using an emission source that shows a positive correlation between the meteo input parameters of the models and the source strength. E.g. for neutral conditions the regression of ratio of the concentrations calculated with FIDES and WindTrax at a height of 0.25m is indicated as $c_{FIDES} = 0.97 \cdot c_{Windtrax}^{0.87}$. For a concentration of 1 the ratio is 0.97 and for a concentration of 100 the ratio becomes 0.53. As the transfer function D in FIDES and WindTrax are only depending on the prevailing turbulent parameters it would be more instructive to use a constant unit emission of 1 and show the ratio on a linear scale as function of u_* and L in a similar way as the authors have done in a previous paper (Carozzi et al., 2013).

We thank A. Neftel and C. Häni for this very useful comment. We propose to modify Figure S3 and section S4.3. Below is given the proposed updated Figure S3 showing the comparison between the two models using linear regressions forced to zero and graphs with linear scales. We propose to change the text in the supplementary material to the following: *In Figure 3, we notice that the concentration modelled with the tuned FIDES at 2 m height was lower by roughly 15% compared to WindTrax under unstable conditions but is comparable under stable and neutral conditions. Lower down at 0.25 m height, the tuned FIDES systematically underestimated the concentration by 15-22% whatever the stability.*

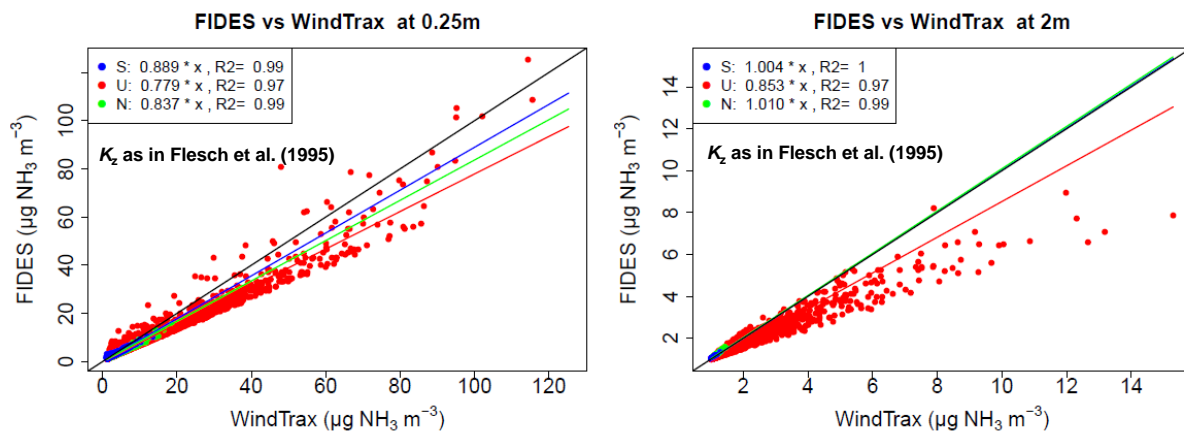


Figure S3. FIDES versus Windtrax concentration modelled above an ammonia source of 25×25 m at 0.25 and 2 m heights. The FIDES vertical diffusivity K_z fits the WindTrax K_z . The comparison is made over the entire year of 2008 in the FR-Gri ICOS site. S, U and N stand for stable, unstable and neutral atmospheric conditions. The linear regression equation is given for each condition together with the R^2 of that regression. The black line is the 1:1 line.

Below we also computed the graphs showing the concentration residual as a function of $1/L$, as suggested by C. Häni and A. Neftel (Figure S4). We propose to include Figure 4 and the following text in the supplementary material: *Figure 4 shows that under unstable conditions FIDES underestimated the concentrations up to 30% at 0.5 m compared to WindTrax, while this gap was reduced and more scattered at 2 m height. Moving towards neutral conditions the two models tend to agree notwithstanding an overestimation of 10% by WindTrax at 2 m height concurrently with an underestimation of the same magnitude by FIDES at 0.5 m. Under stable conditions there was a good agreement at 2 m height, while this agreement remains poorer at lower heights.*

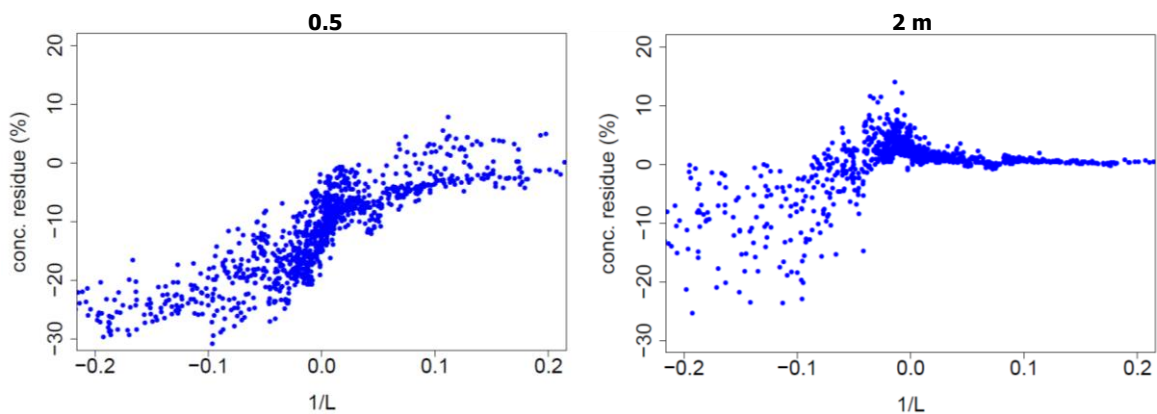


Figure S4. Relative difference between FIDES and WindTrax concentrations as a function of the stability parameter ($1/L$). Data refer to the same conditions reported in Figure S3.

b) Bias related to the concentration measurements

The use of passive diffusive samplers is a challenging business. Within different networks the reliability of PS such as ALPHA samplers or Radiellos have been proven, but the use of them close to emitting source showed major deviations compared to other measurements. E.g. Misselbrook et al. (2005) found severe overestimations of passive diffusive samplers. The latest investigation stems from the Dronten experiment and is discussed in a paper by Michael Bell et al. (submitted to AFM). In this experiment the ALPHA samplers were affected by a positive bias in the order of 50% relative to the other devices. We speculated that the exposure of the PS with the protection hat above them cached eddies from below loaded with higher NH_3 concentrations but shielded eddies with lower concentrations from above. Figure 1 illustrates the NH_3 dynamic that occur over an emitting surface. The concentration was measured with a fast device described in Sintermann et al. (2011). Immediately after application of slurry with a splash plate the NH_3 concentration was measured at a height of 1m above ground with an ionization technique and a strongly heated inlet line to avoid as much as possible damping effects.

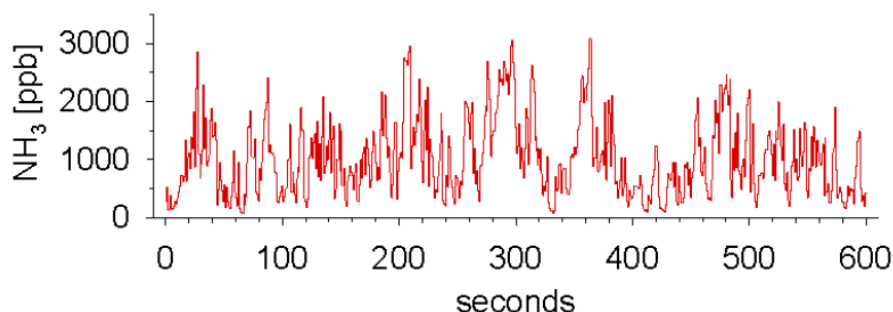


Figure 1: NH_3 concentration time series measured 1m above ground over a manured surface with splash plate.

First we notice as A. Neftel and C. Häni that ALPHA badges are very reliable for network measurements concentrations, as for instance showed by the recent Met-NH₃ project (<http://www.metnh3.eu>). We are however very much aware that the use of ALPHA badges close to emitting sources may be biased. The reason for that bias is however unclear and would need comparisons with fast and unbiased sensors. The assessment by Misselbrook et al. (2005) shows that with high concentrations diffusion samplers may lead to overestimation of up to 70% of the concentration. They suggest potential issues related to the deformation of the Teflon membrane which would modify the distance between coated filters and the Teflon membrane that could cause sampler saturation.

The speculations from A. Neftel and C. Häni are interesting. One could indeed speculate that sweeps, which dominate turbulent transport near the top of the canopy and are characterised by lower wind speed with positive vertical velocity (Poggi and Katul, 2007), could lead to an artificial build-up of the concentration underneath the protecting caps. We could speculate that ejections would not be efficient in “purging” the volume underneath the cap and hence letting over time the concentration being higher in this area. One could also speculate on adsorption-desorption of ammonia on the walls of the ALPHA badges that would be non-linear in response to NH₃ concentrations and lead to possible over estimations under highly fluctuating concentrations as shown in Figure 1 above. This issue necessitates experimental validation of the methodology anyway. We hence propose to add the following text in the discussions section 3.6: *Misselbrook et al. (2005) compared different methodologies and showed that under high concentrations diffusion samplers may lead to overestimation of up to 70% of the concentration. They suggest potential issues related to the deformation of the Teflon membrane which would modify the distance between coated filters and the Teflon membrane that could cause sampler saturation. There is hence some concern on the quality of diffusion samplers to measure concentrations close to large sources which would necessitate field validations.*

We also propose to add a sentence at the end of the conclusion to emphasize this issue for future work: *“Special care should be taken in validating the use of ALPHA samplers near very strong sources”*

Concluding comments:

We judge that the most important potential biases of the proposed multiplot approach are related to biases of the concentration measurements and the used dispersion coefficient. **It would be instructive to calculate probability density functions of the estimated emissions with a dataset that reflect the distributions of the measurements and the turbulence parameters that drive the dispersion model.**

This would indeed be very instructive but we feel that this issue is rather a work to be for a next study. Indeed, in this study we have explored the first order variability which is driven by the change in meteorological conditions observed in the 13 periods over a year in **typical western European climate**. The next step could be to extend this assessment to other datasets part of Fluxnet network to incorporate more continental climate conditions. The script we developed for this study actually incorporates measurement noise but we disabled this feature for calculation time reasons.

The authors have tested their setup in field trial in April 2011 applying slurry with a DM content of 6% and an application rate of 41 kg N-NH₃/ha. According to the details given in the text, we assume that broadband application was used and was compared to fast incorporation and no application. The cumulated loss amounted to 8 to 10% of the applied NH₃. For broadband application, this is a loss on the low side (see e.g. Häni et al.,2016). We would not be astonished if the real emissions would be double as high.

We would like to thank very much A. Neftel and C. Häni for their question and to grant them for their guess. Indeed, we double checked the calculation script used for the real test case and we found one bug in the calculation of the cumulated NH₃ emissions: the multiplicative constant to account for the number of second per time step was set to 30 min while the time step of that particular test case was 60 min. Since a 60 min time step is unusual we did not spot this error in the first place, but we have since then changed the script to calculate the time step from the meteorological dataset. We used this new script and found this bug. This change results in a doubled emission compared to what was given in the discussion manuscript. We hence find, as guessed by A. Neftel and C. Häni that the cumulated losses represented around 20% of the nitrogen applied. We propose to change Figures 16 and 17 as below:

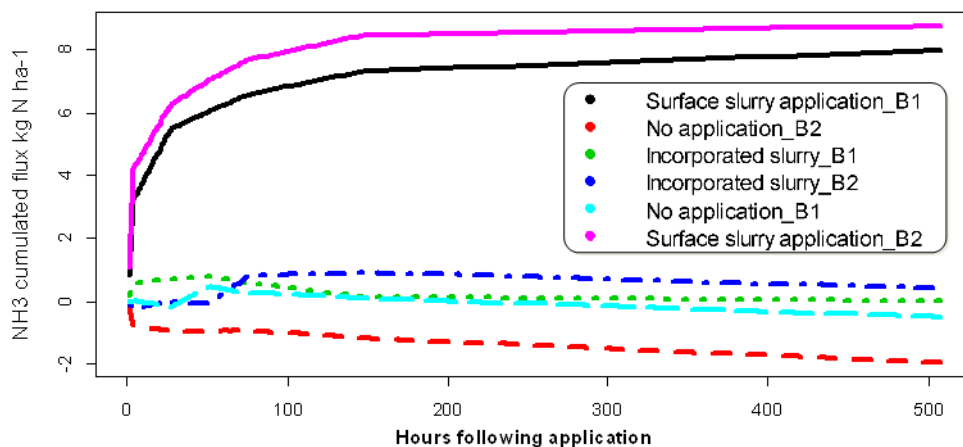


Figure 16. Cumulated fluxes estimated with the inference method on the real test case with strategy C7. Three treatments with two repetitions are compared.

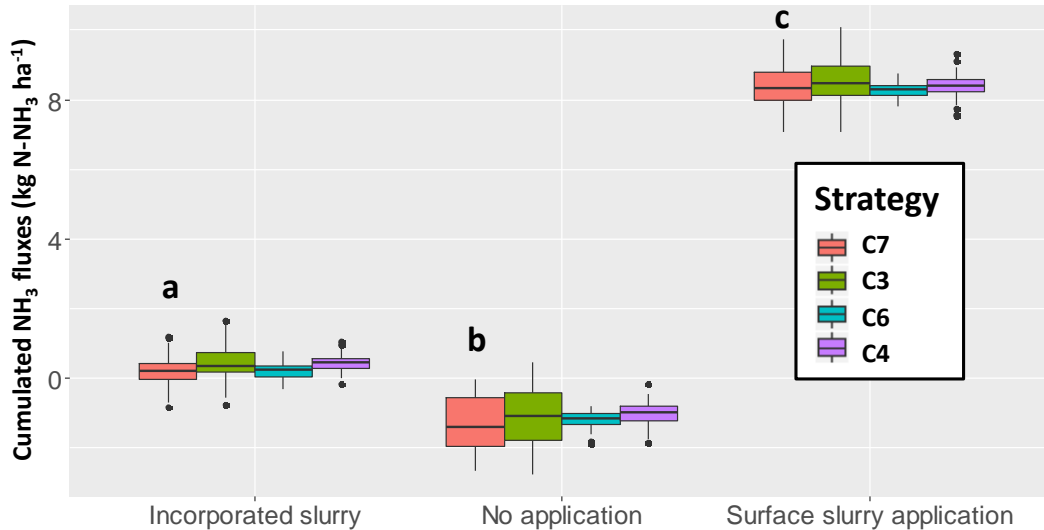


Figure 17. Same as Figure 16 but grouped by treatments and with additional strategies C4 and C6 which consider that replicates have the same surface flux. The variability in the boxplot aggregates the uncertainty on the inference method (the standard deviation on the flux estimate in the least-square model, which accounts for the variability in the replicated concentration measurements), and the variability between the repetitions in each treatment. Letters *a*, *b* and *c* show significant differences between treatments for the C7 strategy, according to a Tukey test (95% family-wise confidence level).

We also propose to modify the text in section 3.5 (lines 630-636) to: *Surface slurry application showed the largest emissions: 9 ± 0.3 kg N ha⁻¹ in B1 and 10 ± 0.2 kg N ha⁻¹ in B2 (median and confidence interval). This corresponds to an emission factor around 23% of the N-NH₄ applied and 8% of the total N applied, which is in-line with agronomic references (Sintermann et al., 2011a; Sommer et al., 2006). In contrast, the incorporated slurry showed much smaller emissions: 0.3 ± 0.2 kg N ha⁻¹ in B1 and 0.6 ± 0.2 kg N ha⁻¹ in B2. It is noticeable that the no-application showed slight deposition, especially in B2: -0.26 ± 0.2 kg N ha⁻¹ in B1 and -1.7 ± 0.2 kg N ha⁻¹ in B2.*

We also propose to change lines 659-663 as follows: *Therefore, we could expect that the real flux is the one measured with C7 times $1.15 (\pm 0.08)$, hence would be 10.9 ± 1.3 kg N ha⁻¹. This corresponds to 27 ± 3 % of the N-NH₄ applied and $\sim 9 \pm 1$ % of the total N applied. For the incorporated slurry, the emissions are around 20 times smaller than the emissions from the surface applied slurry. Under these conditions, the bias on the emission would be around -20%, which means that the corrected emissions would range from 0.5% to 2.5% of the N-NH₄ applied and 0.2 and 0.8% of the total N applied.*

The presented approach to perform NH₃ emission measurements in a multiplot arrangement is encouraging and goes in a good direction. To make the approach more robust, the employed ALPHA NH₃ sampling systems should be validated under real conditions, i.e. over an emitting source in comparison with e.g. MiniDOAS systems (Sintermann et al., 2016).

We completely agree with A. Neftel and C. Häni about this issue. Although the ALPHA badges have shown to be very precise in comparisons under laboratory and field conditions, it is worth comparing

them with an independent technique in a situation where the source is small and intense and where the sensor is placed near the ground (e.g. 50 cm above ground).

Finally, we would like to invite the authors to collaborate with us to compare the FIDES and WindTrax approach. We have an extensive dataset from field trials where we released CH₄ or a mixture of NH₃ and CH₄ from a circular artificial source with a diameter of 20 meters (Häni et al., 2017).

We are honoured by this invitation to collaborate and would be very happy to compare our approach with WindTrax on CH₄ and NH₃ emissions.

References:

- Bell M.W., A. Hensen, A. Neftel, B. Loubet, P. Robin, Y. Fauvel, Y. Hamon, M. Haaima, A.J.C. Berkhout, D.P.J. Swart, W.C.M. van den Bulk, B.F. van Egmond, D. van Dinter, A. Frumau, B. Esnault, C. Decuq, C.R. Flechard Quantifying ammonia emissions from plot-scale and farm-scale sources using integrated mobile measurements and inverse dispersion modelling, (submitted to AFM).
- Carozzi, M., Loubet, B., Acutis, M., Rana, G., Ferrara, R.M., 2013. Inverse dispersion modelling highlights the efficiency of slurry injection to reduce ammonia losses by agriculture in the Po Valley (Italy). *Agric. For. Meteorol.* 171, 306–318. 10.1016/j.agrformet.2012.12.012.
- Flesch, T.K., Wilson, J.D., Harper, L.A., Crenna, B.P., Sharpe, R.R., 2004. Deducing ground-to-air emissions from observed trace gas concentrations: A field trial. *J. Appl. Meteorol.* 43 (3), 487–502.
- Flesch, T.K., Wilson, J.D., Yee, E., 1995. Backward-Time Lagrangian Stochastic Dispersion Models and Their Application to Estimate Gaseous Emissions. *J. Appl. Meteorol.* 34 (6), 1320–1332.
- Häni, C., Sintermann, J., Kupper, T., Jocher, M. and Neftel, A., 2016. Ammonia emission after slurry application to grassland in Switzerland. *Atmospheric Environment*, 125: 92-99.
- Häni, C., Voglmeier, K., Jocher, M., Ammann C., 2017. Recovery rates from line-integrated NH₃ and CH₄ measurements using backward Lagrangian stochastic dispersion modelling. *Geophysical Research Abstracts*, Vol. 19, EGU2017-19557, 2017
- Kormann, R. and Meixner, F.X., 2001. An analytical footprint model for non-neutral stratification. *Boundary Layer Meteorol.*, 99(2): 207-224.
- Misselbrook, T.H., Nicholson, F.A., Chambers, B.J. and Johnson, R.A., 2005. Measuring ammonia emissions from land applied manure: an intercomparison of commonly used samplers and techniques. *Environmental Pollution*, 135(3): 389-397.
- Poggi, D. and Katul, G., 2007. The ejection-sweep cycle over bare and forested gentle hills: a laboratory experiment. *Boundary Layer Meteorol.*, 122(3): 493-515.
- Raupach, M.R., 1987. A Lagrangian Analysis of Scalar Transfer in Vegetation Canopies. *Q.J.R. Meteorol. Soc.*, 113(475): 107-120.
- Raupach, M.R., 1989a. Applying Lagrangian Fluid-Mechanics to Infer Scalar Source Distributions from Concentration Profiles in Plant Canopies. *Agric. For. Meteorol.*, 47(2-4): 85-108.
- Raupach, M.R., 1989b. Stand Overstorey Processes. *Philos T Roy Soc B*, 324(1223): 175-190.
- Raupach, M.R., Legg, B.J., 1984. The uses and limitations of flux-gradient relationships in micrometeorology. *Agricultural Water Management* 8 (1-3), 119–131. 10.1016/0378-3774(84)90049-0.
- Sintermann, J., Dietrich, K., Häni, C., Bell, M., Jocher, M., Neftel, A., 2016. A miniDOAS instrument optimised for ammonia field measurements. *Atmos. Meas. Tech.* 9 (6), 2721–2734. 10.5194/amt9-2721-2016.

- Sintermann, J., Spirig, C., Jordan, A., Kuhn, U., Ammann, C., and Neftel, A.: Eddy covariance flux measurements of ammonia by high temperature chemical ionisation mass spectrometry, *Atmos. Meas. Tech.*, 4, 599–616, doi:10.5194/amt-4-599-2011, 2011.
- Thomson, D.J., 1987. Criteria for the selection of stochastic models of particle trajectories in turbulent flows. *Journal of Fluid Mechanics*, 180: 529-556.
- Wilson, J.D., 2015. Computing the Flux Footprint. *Boundary Layer Meteorol.*, 156(1): 1-14.